12-2021

Ionic Liquid Enhanced Supercritical Fluid Extraction

Kelsey J. Tootle
University of South Alabama, kjt1221@jagmail.southalabama.edu

IONIC LIQUID ENHANCED SUPERCRITICAL FLUID EXTRACTION

A Thesis

Submitted to the Graduate Faculty of the
University of South Alabama
in partial fulfillment of the
requirements for the degree of

Master of Science

in

Chemical Engineering

by
Kelsey Tootle
B. S., University of South Alabama, 2018
December 2021

TABLE OF CONTENTS

Page

LIST OF TABLES

LIST OF FIGURES

Figure Page

LIST OF ABBREVIATIONS

SCF	=	Supercritical Fluid
IL	=	Ionic Liquid
SCFE	=	Supercritical Fluid Extraction
SCFEILE	=	Supercritical Fluid Enhanced Ionic Liquid Extraction
COSMO-RS	=	Conductor-like Screening Model for Real Solvents
PMMA	=	Poly (Methyl Methacrylate)
PR-EOS	=	Peng – Robinson Equation of State
DO1	=	Disperse Orange 1
DENAB	=	4-4’- (Diethylamino) Nitroazobenzene
DR1	=	Disperse Red 1

ABSTRACT

Tootle, Kelsey, M. S., University of South Alabama, December 2021. Ionic Liquid Enhanced Supercritical Fluid Extraction. Chair of Committee: Kevin West, Ph.D.

Supercritical fluids (SCFs) are substances in a state above their critical temperature and pressure ranges where they exhibit some properties of both liquids and gases. This peculiar state generates high transport rates when applied in various chemical processes, in particular, extraction processes. The main limiting factor in using SCFs for extraction is the fact that their moderate solubility leaves room for improvement as most extraction processes are heavily based on relative solubility. The SCF's performance can be enhanced by employing ionic liquids (ILs) – non-volatile liquids composed almost entirely of cations and anions – allowing for the solubility limitation to be circumvented. By taking advantage of SCFs' high transport rate along with ILs' stability, extraction processes will become more efficient and precise. This will lead to developments wherever extraction precision is in demand such as pharmaceutical applications, flavor and fragrance manipulation, or analytical methods. This work explores some of the modeling of solute solubility in the supercritical fluid, screen which ionic liquids as well as presents preliminary experiments

CHAPTER I

INTRODUCTION

Chemical separations are used far and wide for countless processes in the chemical industry and in petroleum refining. From the decaffeination of coffee to the cleaning of water sources to the production of medications, all use a variety of separations. Either a desired substance is freed from a contaminant, or a chosen component is extracted from a larger whole. Both are ways to separate what is wanted from what is not. The research discussed in this thesis focuses on using supercritical fluids in combination with ionic liquids or other non-volatile fluids in extraction processes such as in the latter above, in that the desired component is a much smaller part of a whole. Ideally, the component will be isolated from the whole while leaving both relatively uncontaminated.

Supercritical fluids (SCFs) are substances that have surpassed their critical point – the point above the critical pressure and temperature of the substance. They no longer act as either a liquid or a gas but share some properties of each. The properties remaining in this state lend themselves very well to extractions. The density is high like that of a liquid while the viscosity of the fluid remains low, as seen with gases, which improves transport of the molecules themselves. Both properties can be tuned by adjusting the temperature and pressure of the system. Whether the SCF favors the more gas-like or liquid-like

properties, this peculiar state with heightened diffusivity and lowered viscosity becomes especially advantageous as it generates high transport rates when applied in various chemical processes, in particular, extraction processes. As most extraction processes are heavily based on relative solubility, the main limiting factor in using SCFs for extraction is the fact that their moderate solubility leaves room for improvement. One such improvement is to enhance the SCF's performance by coupling them with ionic liquids in a process that can circumvent the solubility limitation.

Ionic liquids (ILs) – non-volatile liquids composed almost entirely of cations and anions – have been gaining more recognition in the chemical world over the past years. Key features of ILs include low melting points, good solvating ability, high thermal stability, low viscosity, virtually no vapor pressure, and the ability to be modified to display certain selective properties based on the designer's desires. Therefore, an IL with a high affinity for the solute can be designed and utilized. Considering separation systems are based on relative affinity, ILs can provide a driving force by acting as a sink for the SCF to deposit a solute which is in excess of the SCF solubility, thus driving transport into the IL.

If a solid phase substance containing a component that needs to be extracted is placed in a SCF-filled environment that also contains a reservoir or multiple reservoirs of IL(s), the desired component will quickly diffuse into the SCF-rich environment through which it will come into contact with the IL(s). The component, due to its affinity, will readily dissolve into the IL(s). While the component dissolves, its concentration in the SCF will lower, in turn, driving the equilibrium between the solid and SCF to dissolve more solute in the SCF. This creates an incredible mass transfer system in which the

original source and the final solvent do not come into direct contact at all, but instead takes advantage of the SCF as a sort of bridge enabled by the zeroth law of thermodynamics: if substance A (in this case, the desired component) is in equilibrium with substance B (the SCF) while substance B is in equilibrium with substance C (the IL), then substance A is in equilibrium with substance C. In addition, due to the lack of affinity between the SCF and the component, once the system is depressurized there is little, if any, contamination of the SCF meaning it can be recovered completely and reused with little solute being lost.

Although the fundamentals behind this work dates back decades, the application of supercritical fluid to an extraction process involving ionic liquids is still relatively new. By taking advantage of SCFs' high transport rate along with ILs' stability, extraction processes will become more efficient and precise. This will lead to developments wherever extraction precision is in demand such as pharmaceutical applications, flavor and fragrance manipulation, and analytical methods. Due to the energy cost of pressurization, the financial cost of this process could potentially be higher than more common means; however, the advantages could heavily tip the balance in favor of its use.

Before this project is explored, a proof of concept must be established. The main focus of this work is to develop and validate modeling methods and to demonstrate proof of concept experimental extractions to provide sufficient motivation for an NSF proposal. Two types of modeling were developed: the first is a Peng-Robinson cubic equation of state to describe supercritical fluid solubility and second is a COSMO-RS method to evaluate and screen potential ILs and solutes for potentially attractive separations.

CHAPTER II

LITERATURE REVIEW

Ionic liquid enhanced supercritical fluid extraction (ILESCFE as it will be referred to in this paper) takes advantage of the unique properties of both ionic liquids (ILs) and supercritical fluids (SCFs) to efficiently separate a desired component or components from a source. As both ILs and SCFs are highly tunable, finely adjusting the attributes of each provides a way to increase function and performance of experiments or processes. SCFs – fluids above their critical temperatures and pressures – act as vehicles. Similar to how cars take people from one place to another, a SCF is simply a method to transfer contents without retaining them. ILs – salts that are liquid below/ at room temperature – add efficiency to the system by supplying a reservoir not only to collect but to actively draw in the desired component, a reservoir that can be designed to have specific affinities to draw the component out of the solid by driving equilibrium. In this analogy, the desired location is the IL, the people are the component(s)/ solute(s), and the SCF is the vehicle. How much the person desires the new location would also have an impact on how long it took to get there. They don't want to go to work? The trip might be prolonged and take longer just like it would take longer to transfer a component to an IL it does not have an affinity for. One can fine-tune the system by tweaking the properties of either the IL, the SCF, or both to alter the outcome.

Along with tunability and affinity, equilibrium plays a vital role in the transfer as well, because of the zeroth law of thermodynamics: as long as A is in equilibrium with B and B is in equilibrium with C, then C must be in equilibrium with A. If one equilibrium were to shift, then that shift would also shift the other equilibrium. With the IL drawing in the component, there is less in the SCF phase which dissolves more out of the source.

2.1 Supercritical Fluids (SCFs)

A supercritical fluid is a substance that has been heated and pressurized beyond its critical pressure and temperature. The supercritical phase was first observed by Baron Cagniard de la Tour in 1822 (1).

They share properties of both liquids and gases. A SCF typically retains the high density of a liquid but also the low viscosity of a gas. Think of it like a bucket brigade bringing water to fight a fire. The high density allows for higher solvating power allowing the molecules to interact with the desired component much like the people of the human chain being close together allows for a much easier passing of the bucket than if they were far apart. The high transport allows molecule carrying the component to come into contact with another molecule to pass it to. As soon as the bucket of water reaches the next set of hands, it is transferred and that much closer to its destination. In other words, the diffusion of the component through a SCF is much faster and more efficient. These properties make SCFs ideal for mass transport as well as solvating (*Figure 1*). The scale between how much the SCF acts like either a gas or a liquid can also be tuned by adjusting the temperature and pressure.

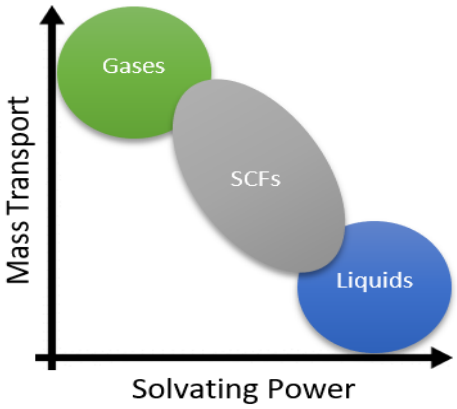

Figure 1.

SCFs have the high mass transport properties of gases and the high solvating power both of which can be fine-tuned by adjusting the pressure and temperature

2.2 Ionic Liquids (ILs)

Ionic liquids were first observed and studied in the late eighteenth century when Friedel and Crafts took note of the "red oil" that come about from their experimentation with aluminum chloride and amyl chloride. About a century later, Japanese chemists identified the red oil was an alkylated aromatic ring cation and a chloroaluminate anion. In 1914, Walden synthesized ethylammonium nitrate which is thought of the "birth of room-temperature ionic liquids." It was not until 1961, that the term "ionic liquids" was coined by Bloom (2).

Liquids are more desirable from a chemistry standpoint as they are more easily manipulated than solids without the struggle of containment that accompanies working with gases. Ionic liquids are salts – composed almost entirely of anions and cations – that are liquid at ambient conditions. Since ILs have a much wider liquid range and will not

evaporate as easily at higher temperatures, they are the ideal material for a chemist. It takes less energy to dismantle the crystalline structure of the solid form of the IL because the ions are large, asymmetric and have lower surface charge densities. As more energy is added, the ions move and vibrate more making their size work against the bonds holding them together. Since less energy is needed to dissolve the solid salts, the melting point is achieved at a much lower temperature (i.e., room temperature) (3).

There is also virtually no limit to what combinations can be created to engineer different properties by changing which ions are used or by mixing multiple ILs together. This gives the designer free reign in deciding which IL to form (2). It gives so many possibilities, in fact, that its generally a good idea to use a software program to sift through or screen for which pairings are most suitable for the project at hand. COSMO-RS is such a screening tool utilized in this work and will be discussed with more detail in a later section.

ILs become even more attractive when you take into account that they have vanishingly low vapor pressure, and they reduce waste since they are more readily recoverable and reusable (2). Everyone from scientists to businesses are always searching for more environmentally friendly alternatives or adjustments to existing practices. Most importantly, people were only given one world. It is better to take care of it when possible. Not to mention, it is good advertising point. It also builds a repertoire with customers and community that the dollar signs are not the only driving force behind business.

2.3 Supercritical Fluid Extraction (SCFE)

The earliest version of SCFE dates back to 1936 when Wilson, Keith and Haylett were refining lubricating oils. Even though the entire process was not under supercritical conditions, they used a liquid near/ around its critical properties to take advantage of the heightened solvating power. SCFE development accelerated in the 1980s. The range and variety of real application extends to everything from extracting flavors and fragrances for foods and perfumes to cleaning electronic parts to nucleation and regulating particle size (1). Diversity of the industries that can benefit from the advancement of SCFE further justifies a deeper exploration into the improvement of current methods.

A substance containing the desired component is placed into a pressure-safe vessel filled and pressurized with a SCF – most commonly CO_2. Once the system is depressurized, the CO_2 can be recovered with very little, if any, solute contamination as opposed to solvents that cannot be easily separated from the solute making them less potent with each use despite possible costly cleaning attempts. Also, although CO_2 will sometimes swell a source (like in the case of the source being a polymer), after depressurization, almost no CO_2 will remain in it. Since the solvent does not need to be replaced, there is less waste meaning less disposal and money is required.

2.4 Polymer Dyeing with Supercritical Fluid

One of the major motivating pieces of literature comes from a previous experiment that took advantage of the supercritical fluid's ability to transport dye solutes from a solid form to a polymer matrix using supercritical CO_2. In the work accomplished by West et. al. polymer poly (methyl methacrylate) (PMMA) and two azo-dyes with

similar affinities for the IL, Disperse Red and 4-4'-(diethylamino) nitroazobenzene (DENAB) were pressurized using supercritical CO_2. The structures of the dyes are as seen in *Figure 2*. This experiment used the same concept as SCFE; however, the polymer dying aimed to insert the solute into the solid polymer instead of removing it. They had complete success as both dyes responded accordingly to dye the polymer (4). The work shown in this research also proves that the higher pressure did, in fact, improve the transfer of the dyes as seen in *Figure 3*.

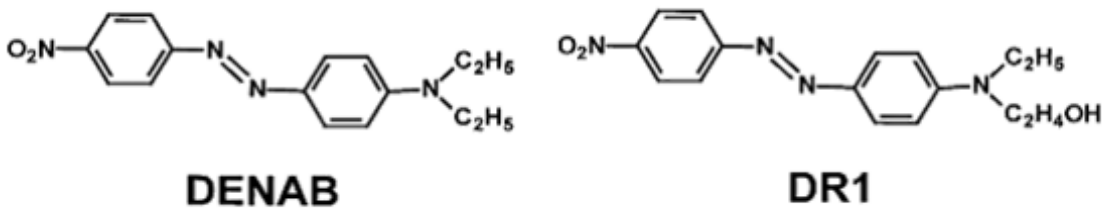

Figure 2.

The molecular structures of the two azo-dyes: DENAB and DR1

Shown in *Figure 3a*, there were differences between the two dyes depending on the affinity and the structure of the dye molecules. As shown in *Figures 3b* and *3c*, DENAB took less time to reach equilibrium than DR1, however, overall there was slightly more DR1 taken up than DENAB (4). This is most likely because DR1 has a slightly higher affinity for the polymer, but the intake of it into the polymer itself was slowed. Perhaps this was due to the structure of the DR1 having a hydroxyl group attached which could have been trying to react with the polymer causing the molecule to

drag along slowing its progress from the surface not allowing more DR1 to take its place, but that is unconfirmed.

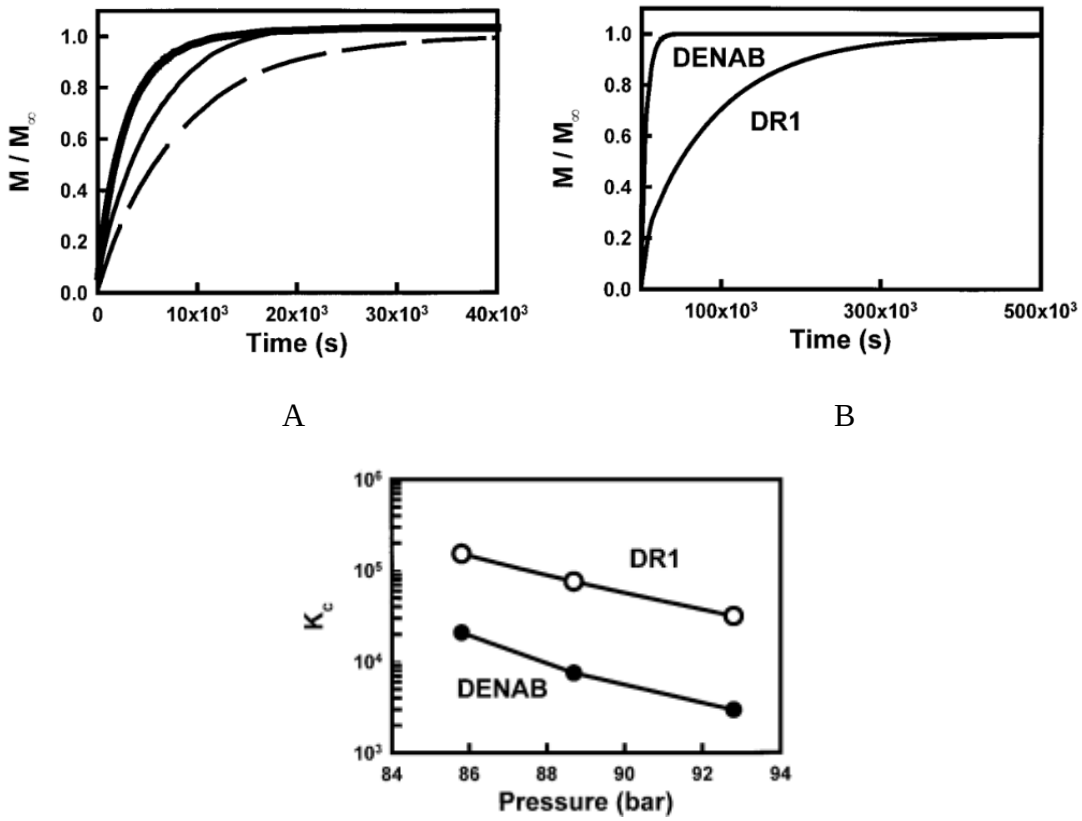

Figure 3.

Uptake of DENAB into the PMMA at 40°C and 88 (dashed), 91 (thin), and 95 (thick) bar; as pressure was increased, diffusion rates and overall absorbance increased is shown in graph *A*. Graph *B* depicts DENAB absorbance compared to DR1 into the PMMA at 40°C and 91 bar; DENAB reached equilibrium much faster than DR1. The last graph shows the overall uptake of DR1 and DENAB over different pressures (*C*).

2.5 Extraction from Ionic Liquids Using Supercritical Carbon Dioxide

Previous work by Blanchard and Brennecke also contributed to the motivation behind looking more closely into coupling the benefits of ILs with SCFs. Blanchard and Brennecke's experiments focused on extraction of various organic products with different types of substituent groups from an IL (1-n-butyl-3-methylimidazolium hexafluorophosphate) using supercritical CO_2. Using the Peng-Robinson equation of state, they estimated the fugacity coefficient in the supercritical phase from the calculated distribution coefficient, *K*. They found that the CO_2 was, indeed, able to completely extract the organic products without contamination from the IL. Even if the IL interacted with a solute, the extent of extraction was not hindered with most reaching 95% extraction or greater. To give a good summary, their closing conclusion statement was: "Overall, ionic liquids and supercritical CO_2 offer not only a new avenue for reactions and separations but have the additional asset of environmental sustainability" (5).

2.6 Enhancing Supercritical Fluid Extraction with Ionic Liquids (SCFEILE)

When the conventional substance used for accumulating the component is replaced with an IL, SCFE becomes even more efficient and tunable. In essence, supercritical fluid enhanced ionic liquid extraction takes all the benefits of SCFE and combines them with the benefits of ILs. The IL acts like a sink as stated above which actively draws in the component, in turn, continuously changing the equilibriums of the system to favor more transfer of the component. According to the zeroth law of thermodynamics, with A (the solute) in equilibrium with B (the SCF) and B in equilibrium with C (the IL), then A is in equilibrium with C (*Figure 4*).

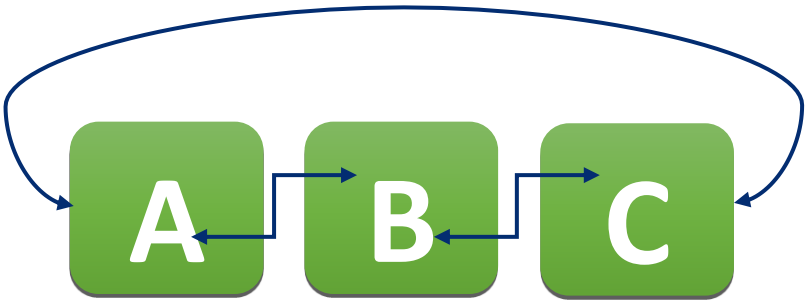

Figure 4.

Zeroth law of thermodynamics where the desired solute (A), is in equilibrium with the SCF (B) and the SCF (B) is in equilibrium with the IL (C); therefore, the desired solute (A) has to be in equilibrium with the IL (C)

Set-up of the SCFEILE was made in the same manner as shown in *Figure 5*. The set-up was slightly changed several times to better accommodate flow or surface area of the substances. These changes are noted in the later experimental section.

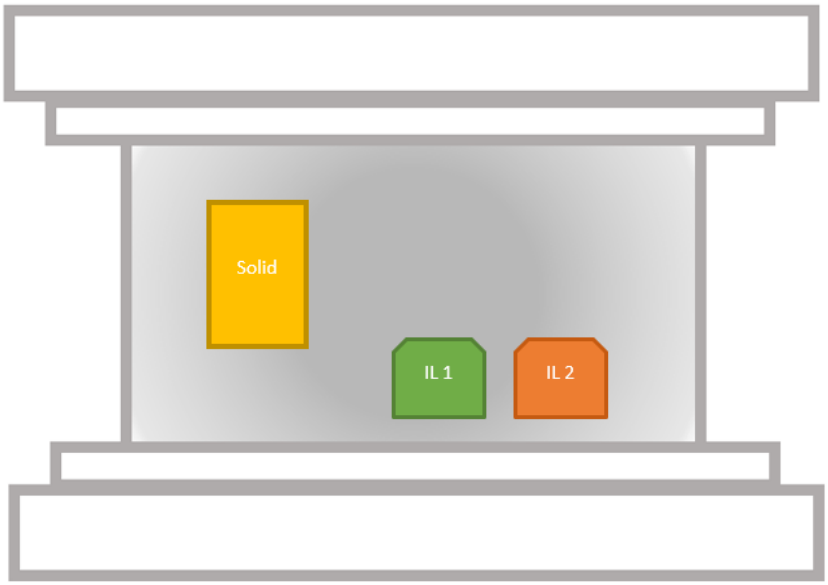

Figure 5.

The solid is placed within a pressure-safe vessel with two ILs. The vessel is then pressurized with a SCF. The desired components are drawn into the SCF and from there, into the IL with its respective affinity.

2.7 COSMO-RS

COSMO-RS stands for Conductor-like Screening Model for Realistic Solvents and is a software that was first published in 1995 (6). It is a method that uses a predictive approach to estimating molecular interactions similar to what group contributions methods (GCMs) use. All of these estimations come from calculating the energy of the interactions (Van der Waals (VdW), Coulomb/ electrostatic and hydrogen bonding) between molecules within the fluid.

Despite the similarities in the basis of both, there are many differences in approach and application of GCMs and COSMO-RS. GCMs are based on functional groupings of the molecule and are heavily reliant on existing experimental data to describe the interactions between the functional groups in specialized situations. They also are intended to be used for ideal fluids such as gases in a vacuum since they are simple molecules influenced almost entirely by the attraction and repulsion of surface-to-surface interactions. These typically only require the short ranged intermolecular forces such as van der Waals in their calculations. More complex fluids such as liquids or gases under less than ideal conditions have greater influence from the longer ranged intermolecular interactions like Coulomb/ electrostatic forces and hydrogen bonding.

COSMO-RS, on the other hand, uses quantum chemical calculations like continuum solvation models (CSMs) coupled with statistical thermodynamics that are used to complete calculations such as chemical potentials, activity coefficients, solubilities, and excess Gibbs free energies to name but a few. The main assumptions COSMO works under ate that the system is in an incompressible liquid state with surfaces in close contact with only pairwise surface interactions.

To obtain the data, COSMO-RS treats mixtures, ILs for instance, as two separate ions instead of one combined substance. It creates an environment like a perfect conductor around the subject molecule (3,7); hence, this is where the "Conductor-like" part of the name comes into play. Whatever effect is needed to neutralize the charge density of the subject molecule is what the 'conductor' shows (*Figure 6*). This is called the screening charge surface which can be broken down into smaller surface segments with their own screening charge σ. For a simple example, if a single water molecule were

to be looked at, the partially positive hydrogens generate a negative screening charges from the "conductor" and the partially negative oxygen generates a positive charge. Employing the conductor's state as a reference state for calculations instead of the usual reference state of an ideal vacuum environment allows for more accurate approximations for solvents and mixtures due to their more complicated influences from their surroundings.

Without relying on existing data, this program can take into account how a "real solvent" would behave as it can take into account the influences of long-range intermolecular forces and the non-idealities of real fluids. This program is a very effective tool in screening for potential solvents or, in this case, which anions and cation to combine to form the ideal ILs.

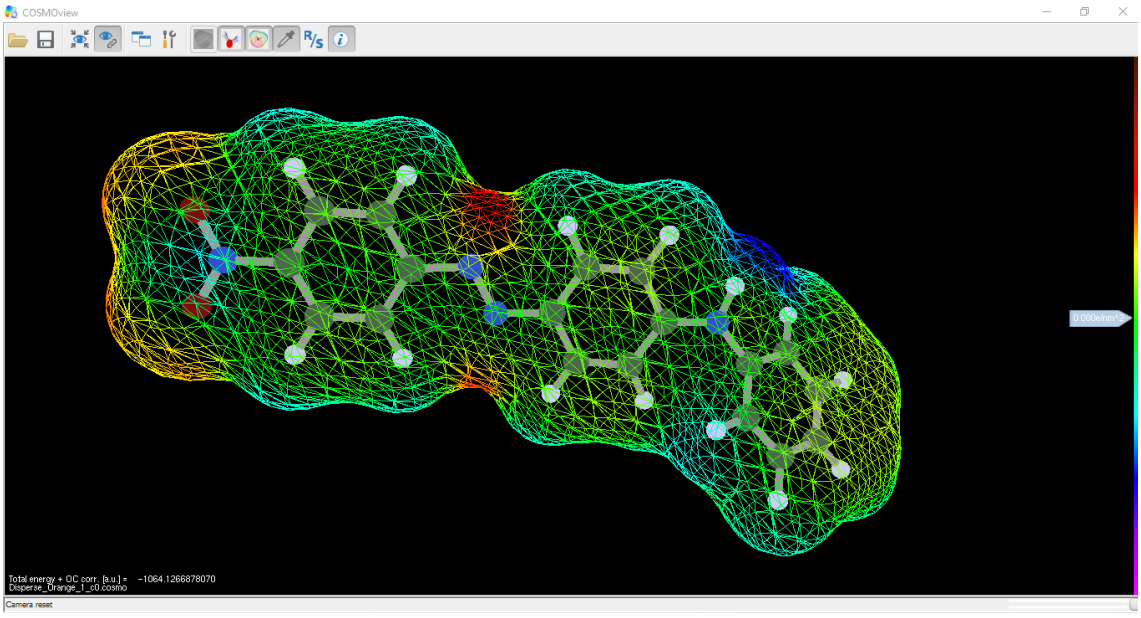

Figure 6.

A Disperse Orange 1 molecule is shown encased in the "ideal conductor" produced by COSMO-RS

At any given moment, each molecule will be in contact with the other molecules in solution meaning a portion or segment of the conductor around a molecule will be in contact with segments of a number of other molecules' conductor segments. Each of these segments have their own screening charge sigma. It is possible that the charges are perfectly opposite, but it is much more probable that there will be differences – or "misfit" energy – between them. This energy can be calculated by *Equations 1* and *2* below.

$$\mathrm{E}_{\mathrm{misfit}(\sigma\cdot\sigma')} = \frac{\alpha}{2}(\sigma + \sigma')^2$$

(*Equation 1*)

$$\mathrm{E}^{\mathrm{total}} = \sum_{\mathrm{x}} \mathrm{E}^{\mathrm{i}}_{\mathrm{ideal}} + \frac{\alpha'}{2}\sum_{\mathrm{v}} \left(\sigma_{\mathrm{v}_1} + \sigma_{\mathrm{v}_2}\right)^2$$

(*Equation 2*)

Besides the misfit interaction, other pairwise surface interaction energies are used to calculate the chemical potential (*Equation 3*) including hydrogen bonding and Van der Waals dispersion forces. There is also a combinatorial term incorporated to express the differences of the size and shape of the segments in contact. The chemical potential is then used to predict the behavior of the molecules in solution (8).

$$\mu_S^X = \mu_{comb}^X + \mu_{disp} + \int p^x(\sigma)\, \mu_S d\sigma$$

(*Equation 3*)

2.8 Tools for Modeling/ Assessing SCFEILE

Extraction processes incorporate a heavy dose of statistical thermodynamics. Namely, the transportation of molecules from one area to another depends on equilibrium, solubilities and ultimately fugacities. Fugacity (f_i) is fundamentally based on Gibbs free energy which accounts for the chemical potential and entropy of a given system.

There are several equilibriums formed in the proposed system. Each IL has its equilibrium with the SCF along with the other IL. COSMO-RS is necessary to model the IL phase while the SCF is described using a cubic EoS – more specifically the Peng-Robinson EoS. COSMO-RS is further utilized to go in depth behind the behavior of the dyes transferred to the PMMA in the paper mentioned in the previous section *2.4 Polymer Dying with Supercritical Fluid*. Much can be learned by examining and coming to understand exactly what is occurring in these different phases.

When multiple phases at the same temperature and pressure are in equilibrium with each other such as it is in this system, their fugacities will be equivalent allowing *Equation 4* to be true.

$$\hat{f}_i^{\,phase\ 1} = \hat{f}_i^{\,phase\ 2} = \ldots = \hat{f}_i^{\,phase\ n} \qquad \text{(Equation 4)}$$

2.8.1 Ionic Liquid – Ionic Liquid

Though they do not physically touch, the ILs are connected through the SCF to establish an equilibrium between each other which will equalize their fugacities (*Equation 5*).

$$\hat{f}_i^{\alpha} = \hat{f}_i^{\beta} \quad \text{(Equation 5)}$$

One can expand the above using *Equation 6* relating the fugacity of a liquid to the Poynting factor (*PF*), saturated pressure (P_i^{sat}), and saturated fugacity coefficient (ϕ_i^{sat}). Once the mole fraction (x_i) and activity coefficient (γ_i) have been incorporated *Equation 7* is realized.

$$f_i = \phi_i^{sat} P_i^{sat} PF \quad \text{(Equation 6)}$$

$$x_i^{\alpha} \gamma_i^{\alpha} \phi_i^{sat} PF\ P_i^{sat} = x_i^{\beta} \gamma_i^{\beta} \phi_i^{sat} PF\ P_i^{sat} \quad \text{(Equation 7)}$$

where $PF = \exp\left(\frac{V_i^l (P - P_i^{sat})}{RT}\right)$

Since the fugacity coefficient, Poynting factor, and saturated pressure are the same for either side, they cancel each other out leaving *Equation 8*.

$$x_i^{\alpha} \gamma_i^{\alpha} = x_i^{\beta} \gamma_i^{\beta} \quad \text{(Equation 8)}$$

Rearranging the above to place the mole fractions on the left gives a ratio of the activity coefficients on the right of *Equation 9*. This is how the selectivity is determined later on in section 4.1.1 since the ratio of the activity coefficients are equal to the inverse of the mole fractions.

$$\frac{x_i^a}{x_i^\beta} = \frac{\gamma_i^\beta}{\gamma_i^\alpha} \qquad \text{(}\textit{Equation 9}\text{)}$$

2.8.2 Ionic Liquid – Supercritical Fluid

A requisite before acting as a bridge between the ILs, is the equilibrium between the SCF and each IL must be formed. Again, one can use *Equation 5* to set the fugacity of the SCF (s) equal to the ionic liquid (l) as shown in *Equation 10*:

$$\hat{f}_i^s = \hat{f}_i^l \qquad \text{(}\textit{Equation 10}\text{)}$$

This time, however, is not between two liquids so the SCF is described not from *Equation 6*, but from this fugacity equation:

$$\hat{f}_i^v = y_i \hat{\phi}_i P \qquad \text{(}\textit{Equation 11}\text{)}$$

Substituting in the above equation gives:

$$y_i \hat{\phi}_i P = x_i \gamma_i \phi^{sat} PF \; P_i^{sat}$$ (*Equation 12*)

The right side describes the IL as it did in *Equation 6,* and the left side uses the vapor mole fraction (y_i), solution fugacity coefficient ($\hat{\phi}_i$), and pressure (P) to describe the SCF.

CHAPTER III

METHODS

3.1 Experimental

Of the many combinations of separation situations, the main ones to focus on for this research are an enhanced extraction from a matrix by a single IL, the separation of two different solutes from a mixture by two different ILs, and ultimately, how to apply this method to industrial applications.

Foremost, this work aims to verify that SCFEILE will apply to extraction processes in general and further, that it is a more efficient/ cleaner approach than traditional methods due to the driving force provided by the IL from shifting equilibriums to favor the solute uptake. Several physical experiments have been completed to this effect as shown later in the Results section. More experiments will be carried out to test factors that have not yet been studied.

After this has been achieved, additional experiments will be conducted to establish that given a system with two desired components (C1 and C2) intermixed, an individual will be able to first separate both mixtures from the original matrix into the SCF. Once the components are in the SCF, two different ILs (IL1 and IL2) will be used to separate them from each other. If IL1 has an affinity for C1 and IL2 has an affinity for

C2, then each component will be drawn toward its respective IL. Thus, the components have been extracted from the original matrix and separated from the other.

3.2 Modeling

Two different types of modeling are used. One utilizes the Peng-Robinson equation of state (*Equation 14*) (9) and quadratic mixing rules (*Equation 15* and *16*) (10, 11) set up in Microsoft Excel using visual basic coding to calculate compressibility factors, densities, and interaction coefficients to determine the solubilities of the dyes into the selected SCF. The other puts to work the software COSMO-RS to sift through various cation and anion pairings to determine which are best suited to be used as a specific experiment's ILs based on the calculated activity coefficients.

3.2.1 Solubility Modeling

The ideal gas equation (*Equation 13*) shows the basic relationship between pressure (P), temperature (T), and volume (V) as they apply to an ideal gas in perfect vacuum conditions. R represents the gas constant. The equation works under the assumptions that the molecules in question are small, perfect spheres that take up very little volume and possess no or negligent attractive and repulsive intermolecular forces between them.

$$P = \frac{RT}{V} \qquad \text{(Equation 13)}$$

General cubic equations of state (EoS) take the form of *Equation 14*. They introduce the temperature dependent variable *a(T)* to account for interactions that attract or pull the molecules closer together and the variable *b* for the ones that repel or push the molecules away from each other. Epsilon (ϵ) and sigma (σ) are both parameters that are given depending on which EoS is used along with ψ (shown in *Equation 18*) and Ω (shown in *Equations 18* and *19*). The values used for Peng-Robinson are given in *Table 1*. Since this work uses ILs which are mixtures of two molecules, the a and b terms become mixture terms as defined by the mixing and combining rules in *Equations 15* and *16*. The k_{ij} and l_{ij} terms are interaction coefficients determined from experimental data. These parameters describe the experimental strength of the intermolecular interactions compared to their geometric mean. They can range from -1 to 1 with values > 0 meaning interactions between unlike molecules are weaker than the geometric mean would suggest and values < 0 meaning they are stronger than the mean.

$$P = \frac{RT}{V-b} - \frac{a(T)}{(V+\epsilon b)(V+\sigma b)} \quad \text{(Equation 14)}$$

$$a = \sum_i \sum_j x_i x_j a_{ij} \quad where \;\; a_{ij} = \left(a_{ii} a_{jj}\right)^{1/2}\left(1 - k_{ij}\right) \quad \text{(Equation 15)}$$

$$b = \sum_i x_i b_i \quad \text{(Equation 16)}$$

Table 1. Peng-Robinson Parameter Table (9)

Parameter	σ	ϵ	Ω	ψ
Value	$1+\sqrt{2}$	$1-\sqrt{2}$	0.07780	0.45724

Visual Basic was used to program the Peng-Robinson (PR) EoS (9) into Excel. The main reason PR was chosen is because it has higher accuracy paired with less complex computations which allows for relatively fast and reliable calculations. Its accuracy can be partially attributed to the use of an acentric factor (ω) as an additional parameter to take into consideration the non-sphericity of molecules. *Equation 17* shows how it is incorporated into the calculations for an empirical alpha ($\alpha(T_r)$) equation (*Equation 19*). *Equation 19* is then worked into *Equation 20* which generates a *q* term that will be used in conjunction with a β term (*Equation 21*) to manipulate the general cubic EoS to develop a usable compressibility factor equation (*Equation 20*).

$$\alpha(T_r,\omega)=\left[1+(0.37464+1.54226\omega-0.26992\omega^2)\left(1-T_r^{\frac{1}{2}}\right)\right]^2 \qquad (\textit{Equation 17})$$

$$q=\frac{a(T)}{bRT}=\frac{\psi\alpha(T_r)}{\Omega T_r} \qquad (\textit{Equation 18})$$

$$\beta=\frac{bP}{RT}=\Omega\frac{P_r}{T_r} \qquad (\textit{Equation 19})$$

$$Z=1+\beta-q\beta\frac{Z-\beta}{(Z+\epsilon\beta)(Z+\sigma\beta)} \qquad (\textit{Equation 20})$$

The compressibility factor can then be used to calculate the residual Gibbs free energy (*Equation 21*). A property that can be employed to determine the fugacity coefficient (ϕ) of any species even when not under ideal conditions.

$$\frac{G^R}{RT} = Z - 1 - \ln(Z\beta) - qI = ln\ \phi_i \qquad \text{(Equation 21)}$$

Although the fugacity of different states of matter are calculated differently, when the system is at equilibrium, the natural logarithm of each phase's fugacity coefficient is equal to each other (*Equation 22*). This creates a condition that allows

$$ln\phi_i^v = ln\phi_i^L = ln\phi_i^{sat} \qquad \text{(Equation 22)}$$

3.2.2 COSMO-RS

COSMO-RS is the other modeling method. This model can screen through a wide range of possible anions and cations to make the most ideal combination for an IL. It will allow for a selection or selections of the most favorable IL(s) by calculating activity coefficients (γ_1) to compare using a modified Raoult's Law as shown in *Equation 23.*

$$y_\mathrm{i} = \frac{x_\mathrm{i}\gamma_\mathrm{i}P_\mathrm{i}^{sat}}{P} \qquad \text{(Equation 23)}$$

CHAPTER IV

RESULTS

4.1 Modeling

4.1.1 COSMO-RS

Exploration has been made into the COSMO-RS programs such as COSMOThermX which calculated the activity coefficients used to create the sample thermal graph shown in *Figure 7*. If one had the desire to selectively separate a solute, aspirin in this case, from a source with another desired solute, this graph would be used to select the sets of ILs with the most difference between them. That is assuming that the IL pairing not favoring the aspirin would favor the other desired solute. In the case of this graph, the cation/ anion pair making up the IL of the top left corner (the smallest value) and the pair making the bottom right IL (the largest value) would be chosen as they have the greatest difference in values. The greater difference in their values would generate a greater selectivity (*Equation 9*) of the solutes between the ILs.

	A1	A2	A3	A4	A5	A6	A7	A8	A9	A10
C1	209.44	14.80	17.47	14.50	13.98	13.44	12.97	12.61	19.69	15.22
C2	118.93	7.07	8.96	7.17	6.57	6.25	6.00	5.83	7.76	5.11
C3	6.72	7.65	7.58	8.22	7.68	7.72	7.71	7.68	4.60	3.36
C4	7.11	7.04	6.93	7.59	7.06	7.10	7.10	7.08	3.88	2.69
C5	6.94	7.12	7.00	7.66	7.15	7.19	7.18	7.16	4.13	2.98

Figure 7.

Activity coefficients were calculated for the aspirin in 50 combinations of cation/anion (5 anions and 10 cations) pairings. The results of each pairing were placed in excel and conditional formatting was used to provide a gradient for the numerical values. The smallest values are more red in color and the greatest values are more green while the middling values have a yellow coloring.

Not only does COSMOThermX calculate activity coefficients, it also allows one to directly calculate the selectivity of one component over another in a given IL. Use of this application to analyze the selectivity of DR1 over DENAB in PMMA, allowed *Figure 8* to be created. This figure gives a quick visual representation of which cation/ anion pairings create more effective ILs.

From analysis of the data, patterns can be seen in the thermal graph shown in *Figure 8*. Isolating certain key aspects that create these patterns show the influence each has over the selectivity. Once the influence is known, it can be used to possibly predict better combinations of cations and anions for more productive ILs. Most of the influence seen in this system is due to the polarity of the IL interacting with the hydroxyl group on the DR1 molecule. More specifically, the charge density or “hardness” of the anion in the IL is the driving force behind the patterns seen. Though there are also patterns within the cations, the anions have a much more drastic impact on the selectivity; therefore, the

overall graph was segmented into three sections based on anion groupings. *Figures 9* through *11* highlight the patterns within these groupings.

c/a	A1	A2	A3	A4	A5	A6	A7	A8	A9	A10	A11	A12	A13
C1	2.6	2.0	9.9	21	25	15	48	73	21	59	161	1343	14099
C2	3.5	2.4	12.0	21	26	15	45	65	21	53	136	949	7942
C3	2.4	1.9	8.9	18	21	13	38	57	19	50	132	953	8374
C4	1.9	1.6	7.5	18	21	13	42	65	18	54	156	1359	15340
C5	2.1	1.7	7.7	16	19	12	35	54	17	46	124	914	8230
C6	1.9	1.6	6.8	15	18	11	33	50	16	43	117	869	7978
C7	1.6	1.5	6.0	14	16	10	31	47	14	40	109	817	7614
C8	1.5	1.4	5.4	13	15	10	28	44	13	37	101	770	7289
C9	3.7	2.5	12.1	24	29	17	53	79	22	58	146	1154	10974
C10	2.8	2.1	10.4	23	28	16	53	81	22	64	172	1511	16628
C11	2.5	2.0	9.3	20	24	15	47	71	21	60	158	1334	13745
C12	2.0	1.7	8.1	20	23	14	46	72	20	62	170	1546	17732
C13	1.7	1.6	7.1	18	21	13	42	67	19	58	162	1495	17526
C14	1.5	1.4	6.3	17	19	12	40	63	17	54	153	1435	17195
C15	1.4	1.3	5.6	15	18	12	37	60	16	51	144	1368	16724
C16	3.1	2.2	11.1	23	28	16	51	76	22	60	155	1250	12136
C17	2.5	2.0	9.5	22	26	16	51	80	22	66	180	1629	18859
C18	2.0	1.8	8.3	20	24	15	48	76	21	65	182	1702	20428
C19	1.8	1.6	7.3	19	22	14	45	71	19	62	174	1648	20113
C20	1.6	1.5	6.5	17	20	13	42	67	18	58	166	1593	19937
C21	1.4	1.4	5.8	16	19	12	39	63	16	54	155	1498	18908
C22	1.2	1.3	5.2	15	17	11	36	59	15	50	146	1427	18431
C23	1.1	1.2	4.7	14	16	11	34	56	14	46	136	1345	17469

Figure 8.

Selectivity of disperse dye DR1 over disperse dye DENAB in the PMMA were calculated in various ionic liquids. Each column contains a different anion (A1-A13) and each row has a different cation (C1-C23). Every cell is a hypothetical ionic liquid composed of the anion of the column and the cation of the row it occupies. A list of the cations and anions can be found below in *Table 2*.

Table 2.

A list of the cations and anions used in *Figures 10-13*. The cations are separated into imidazoliums, pyrrolidiniums, and piperidiniums. The anions are separated into fluorous, alkylated sulfates, and halides.

Cations		Anions	
C1	1-ethyl-3-methyl-imidazolium	A1	PF_6
C2	1-ethyl-2,3-dimethyl-imidazolium	A2	TFSI
C3	1-butyl-3-methyl-imidazolium	A3	BF_4
C4	1-butyl-2,3-dimethyl-imidazolium	A4	Butylsulfate
C5	1-pentyl-3-methyl-imidazolium	A5	Ethylsulfate
C6	1-hexyl-3-methyl-imidazolium	A6	Octylsulfate
C7	1-heptyl-3-methyl-imidazolium	A7	Tosylate
C8	1-octyl-3-methyl-imidazolium	A8	Hexylsulfate
C9	Dimethyl-pyrrolidinium	A9	Iodide
C10	Methyl-ethyl-pyrrolidinium	A10	Bromide
C11	Methyl-(2-methoxyethyl)-pyrrolidinium	A11	Chloride
C12	Methyl-butyl-pyrrolidinium	A12	Sulfate
C13	Methyl-pentyl-pyrrolidinium	A13	Flouride
C14	Methyl-hexyl-pyrrolidinium		
C15	Methyl-heptyl-pyrrolidinium		
C16	Dimethyl-piperidinium		
C17	Methyl-ethyl-piperidinium		
C18	Methyl-propyl-piperidinium		
C19	Methyl-butyl-piperidinium		
C20	Methyl-pentyl-piperidinium		
C21	Methyl-hexyl-piperidinium		
C22	Methyl-heptyl-piperidinium		
C23	Methyl-octyl-piperidinium		

c/a	A9	A10	A11	A12	A13
C1	21	59	161	1343	14099
C2	21	53	136	949	7942
C3	19	50	132	953	8374
C4	18	54	156	1359	15340
C5	17	46	124	914	8230
C6	16	43	117	869	7978
C7	14	40	109	817	7614
C8	13	37	101	770	7289
C9	22	58	146	1154	10974
C10	22	64	172	1511	16628
C11	21	60	158	1334	13745
C12	20	62	170	1546	17732
C13	19	58	162	1495	17526
C14	17	54	153	1435	17195
C15	16	51	144	1368	16724
C16	22	60	155	1250	12136
C17	22	66	180	1629	18859
C18	21	65	182	1702	20428
C19	19	62	174	1648	20113
C20	18	58	166	1593	19937
C21	16	54	155	1498	18908
C22	15	50	146	1427	18431
C23	14	46	136	1345	17469

Figure 9.

Halogen anion group: iodide, bromide, chloride, sulfate, and fluoride. The highest selectivity within this group is 20,428 (C18A13) and the least is 13 (C8A9).

c/a	A1	A2	A3
C1	2.6	2.0	9.9
C2	3.5	2.4	12.0
C3	2.4	1.9	8.9
C4	1.9	1.6	7.5
C5	2.1	1.7	7.7
C6	1.9	1.6	6.8
C7	1.6	1.5	6.0
C8	1.5	1.4	5.4
C9	3.7	2.5	12.1
C10	2.8	2.1	10.4
C11	2.5	2.0	9.3
C12	2.0	1.7	8.1
C13	1.7	1.6	7.1
C14	1.5	1.4	6.3
C15	1.4	1.3	5.6
C16	3.1	2.2	11.1
C17	2.5	2.0	9.5
C18	2.0	1.8	8.3
C19	1.8	1.6	7.3
C20	1.6	1.5	6.5
C21	1.4	1.4	5.8
C22	1.2	1.3	5.2
C23	1.1	1.2	4.7

Figure 10.

Fluorous anion selection: PF_6, TFSI, and BF_4. The highest selectivity within this group is 12.1 (C9A3) and the least is 1.1 (C23A1).

c/a	A4	A5	A6	A7	A8
C1	21	25	15	48	73
C2	21	26	15	45	65
C3	18	21	13	38	57
C4	18	21	13	42	65
C5	16	19	12	35	54
C6	15	18	11	33	50
C7	14	16	10	31	47
C8	13	15	10	28	44
C9	24	29	17	53	79
C10	23	28	16	53	81
C11	20	24	15	47	71
C12	20	23	14	46	72
C13	18	21	13	42	67
C14	17	19	12	40	63
C15	15	18	12	37	60
C16	23	28	16	51	76
C17	22	26	16	51	80
C18	20	24	15	48	76
C19	19	22	14	45	71
C20	17	20	13	42	67
C21	16	19	12	39	63
C22	15	17	11	36	59
C23	14	16	11	34	56

Figure 11.

Sulfates with alkyl groups anion selection: butylsulfate, ethylsulfate, octylsulfate, tosylate, and hexylsulfate. The highest selectivity within this group is 81 (C10A8) and the least is 10 (C7A6 and C8A6).

Overall, the most notable pattern on the main chart is that the extreme values are on the right and left sides. The highest selectivities are seen on the right side where the ILs have single atom halogens or the small molecule sulfate as the anion. This makes sense because their charge densities are concentrated around them making them "hard" anions. This makes them more attracted to the polar DR1, because the partial positive charge on the hydroxyl group of the DR1 will interact with the negative charge of the anion. The stronger the concentration of that negative charge, or the higher the "hardness" of the anion is, the stronger the interaction between them will be. On the left side are the least selective of the subsets. The fluorous anions (PF6, TFSI, BF4) do not have that concentrated charge, but rather their charges are spread out around the ions. In other words, these are "soft" anions. The anions of the middle group between these extremes do have a polar end but the nonpolar tails draw that charge energy away from it spreading the charge out. This keeps the anions from being "hard" or "soft", and the IL pairings from being as attractive.

4.1.2 COSMO-RS Application – PMMA Solubility

From the graphs above and the journal article discussed in section 2.4 of this paper, one can get the general idea of the solubility of the disperse dyes in the PMMA along with some of the more in-depth reasoning behind it. However, more could be done to better understand how each of the dye molecules interacts with the PMMA's. To build on what West et al. accomplished, this research further delved into understanding the transport of the dyes into the PMMA using COMSO-RS to model the activity coefficients under similar conditions to those of the paper.

With the temperature kept at 40°C, different weight percentages were used based on the paper by Liu et al (12). This was done to simulate the CO_2 that is present in the PMMA from swelling at different pressures. The pressures 70, 80, 90, and 100 bar were chosen because they correspond to the change of rate in the graph of *Figure 12* which leads up to the point CO_2 becomes supercritical. *Figure 13* shows the activity coefficients calculated at these conditions and *Table 3* shows what mass fraction of CO_2 in the PMMA corresponds to what pressure.

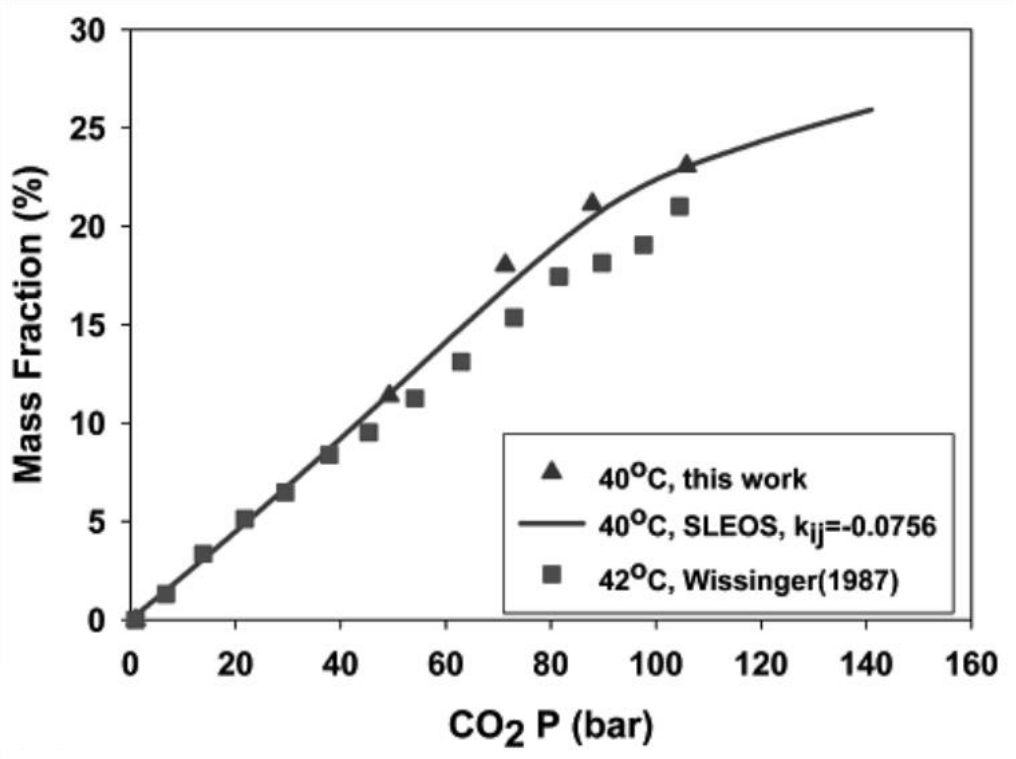

Figure 12.

This graph shows the uptake of CO_2 by the swollen PMMA as determined by three methods: experimentation by Liu et. al., calculated using the Sanchez-Lacombe equation of state, and as found in literature by Wissinger. This figure was taken from the work done by Liu et. al. (12)

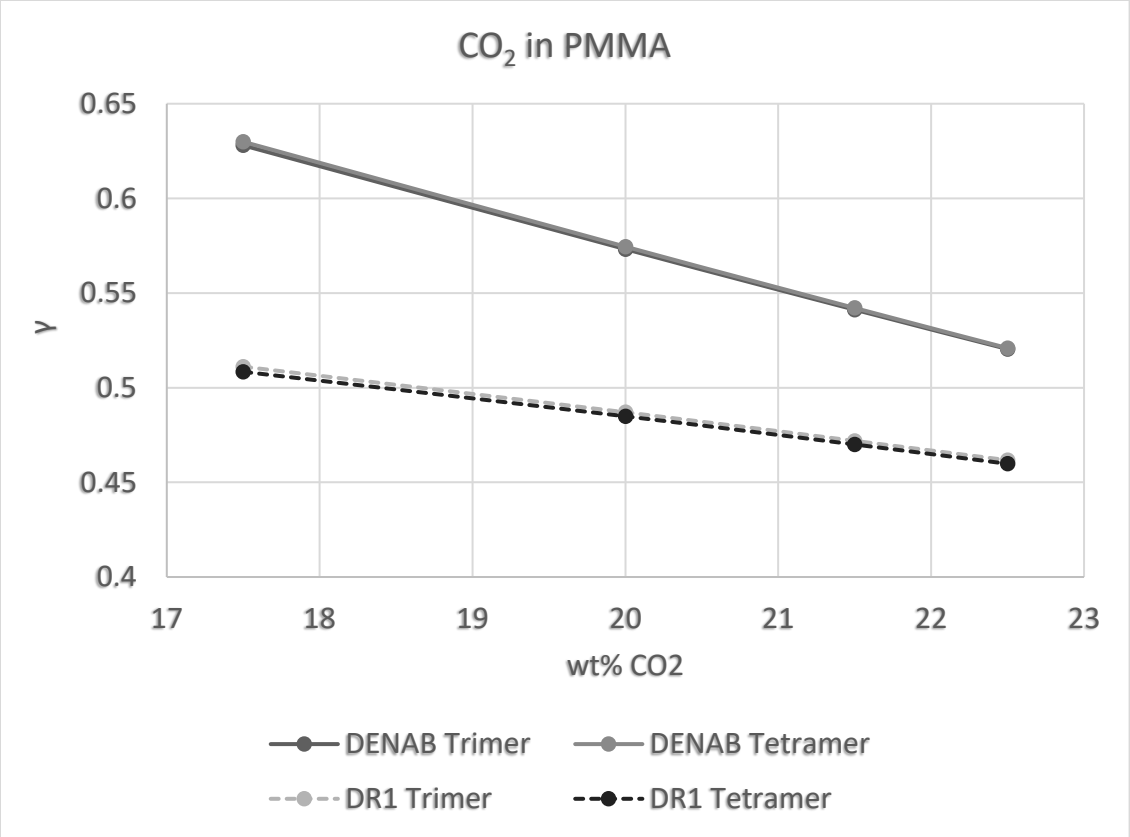

Figure 13.

Activity coefficients of disperse dyes DENAB and DR1 into PMMA as a tetramer and as a trimer at different weight percentages of CO_2 that correspond to different temperatures as shown in *Table 2* (12).

Table 3. Mass Fraction of CO2 and Its Corresponding Pressure

Mass Fraction	Equivalent Pressure
17.5	70 bar
20.0	80 bar
21.5	90 bar
22.5	100 bar

4.1.3 Solubility Modeling

Excel was set-up with a VBA code (see Appendix A for code) to fit the parameters of the Peng-Robinson equation of state with the mixing rules in *Equations 15* and *16*. An interaction parameter (k_{ij} of *Equation 15*) was solved for using experimental values of literature (13) at 4 different temperatures. The values were then fit to a curve to allow for a more predictive equation that could be applied to various temperatures. The fit k_{ij} equation was then used to iteratively calculate the concentration of the solute in the solvent. The following two models were made using this code.

Knowing how the density and the compressibility of carbon dioxide (the chosen SCF for this work) helps to understand the behavior of the gas as the temperature and pressure increase inside the system. From the graph in *Figure 14*, a great deal of information can be gathered. First, the effects of increasing the temperature are decreased density and increased compressibility. Second, increasing the pressure increases the density, of course. The compressibility factor decreases until the molecules begin to get so close that the repulsive intermolecular forces begin to dominate the attractive forces which forces the compressibility factor to begin to increase once more. An interesting thing to take note of is that there is a steep increase in density around the same pressure that the compressibility factor begins to increase.

To determine the effects of temperature and pressure on the solubility in carbon dioxide, solubility curves were calculated up to 300 bar at four temperatures. Caffeine was used as the solute in the modeling as it is a very common component to many everyday foods, drinks and medicines and it is one of the main subjects in a proposed future application as described later on. In the graph (*Figure 15*), the solubility drastically

increases over the same range seen in *Figure 14* to have steep increase of density and a change from decreasing to increasing compressibility. This is the point at which increasing the pressure provides much less increase in efficacy of the extraction. This helped to decide at which pressure and temperature the experiments discussed later were run at.

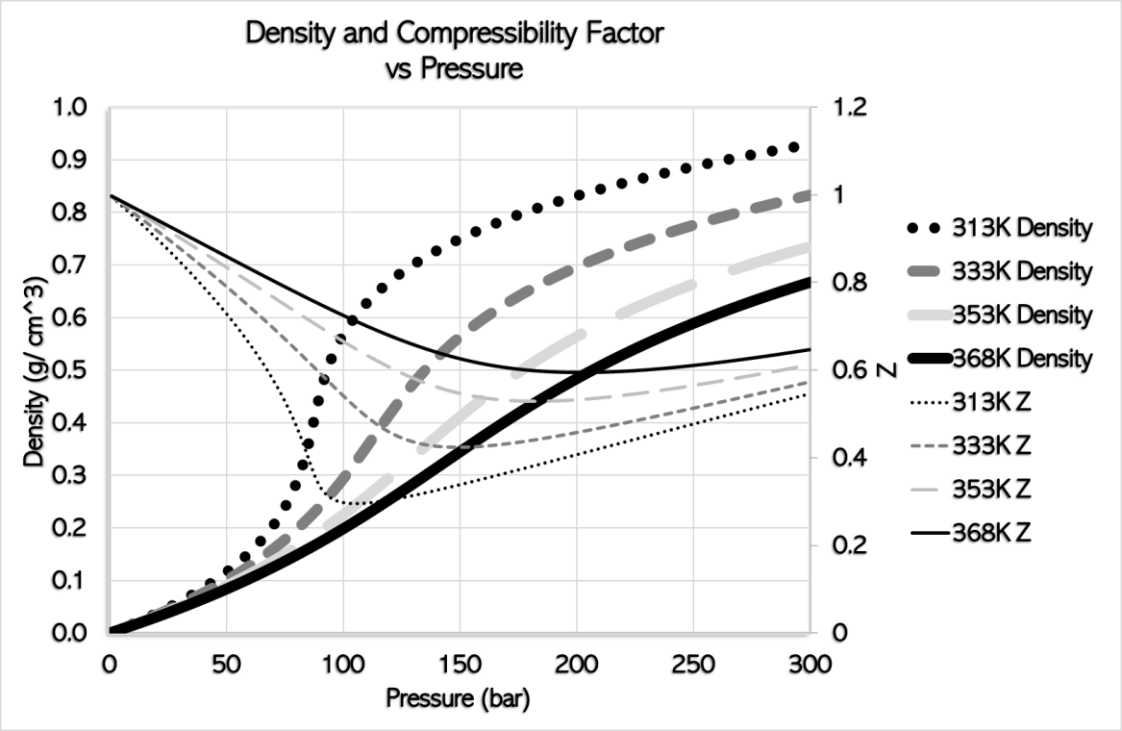

Figure 14.

Comparison of caffeine's density and compressibility factor in supercritical carbon dioxide is given at four different temperatures including 313K, 333K, 353K and 368K.

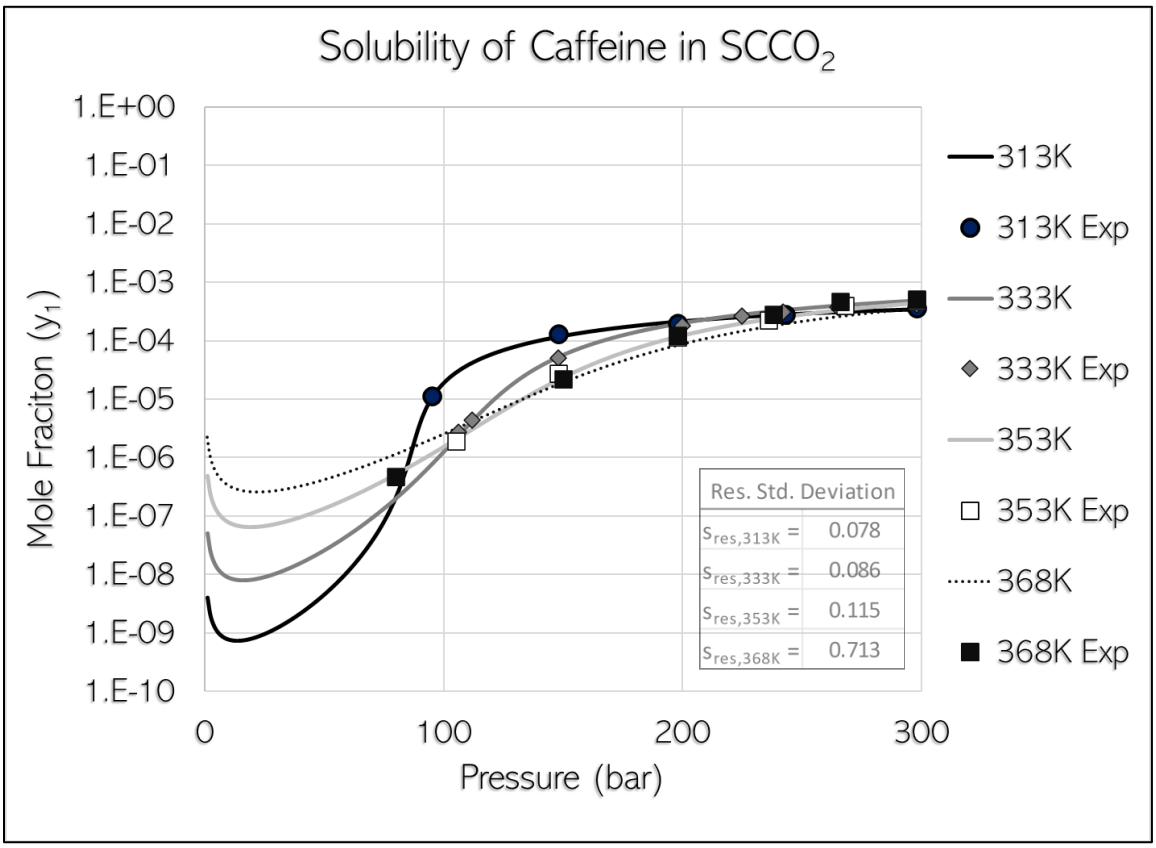

Figure 15.

The solubility of caffeine in supercritical carbon dioxide given at four different temperatures including 313K, 333K, 353K and 368K (13).

4.2 Experimental

4.2.1 List of Experiments

Table 4. List of Experiments

Series	Exp #	Description	Fundamental Theory
Preliminary Proof of Concept (40oC)	1	Transfer of solid dye to IL	Zeroth Law
	2	Transfer of dye from IL to same IL – 4 days	
	3	Transfer of dye from IL to same IL w/ mixing – 1 day	Effective Time
	4	Transfer of dye from IL to same IL w/ mixing – 2 days	
	5	Transfer from mixed solid dye to IL	Selective Transfer
	6	Selective Transfer to one IL over another	
	7	Transfer from filter paper to IL	Transfer from a matrix
	8	Citric acid and water Co-transfer	Transfer to a non-IL
Time (40°C)	9	Selective transfer of solid dye – 6 hr	Time dependence of selective transfer of solid dye
	10	Selective transfer of solid dye – 12 hr	
	11	Selective transfer of solid dye – 3 hr	
	12	Selective transfer of solid dye – 6 hr (redo of Exp 9)	
	13	Selective transfer of solid dye – 1.5 hr	
Temp (60°C)	14	Selective transfer of solid dye – 6 hr	Temperature dependence of selective transfer of solid dye
	15	Selective transfer of solid dye – 24 hr	
	16	Selective transfer of solid dye – 1.5 hr	
Shikimic Acid Series	17	Soxhlet Extraction	Soxhlet Extraction
	18	Transfer of powdered shikimic acid to water -3 hrs	Transfer of powdered shikimic acid to water
	19	Transfer of powdered shikimic acid to water -6 hrs	
	20	Transfer from ground star anise to water	Transfer from natural SA source to water

4.2.2 Equipment and General Procedure Used:

Each experiment began by filling an iSCO 500D syringe pump with CO2 and loading a Parr reactor with the experiment and sealing it before placing it in a temperature-controlled jacket (*Figure 16*).

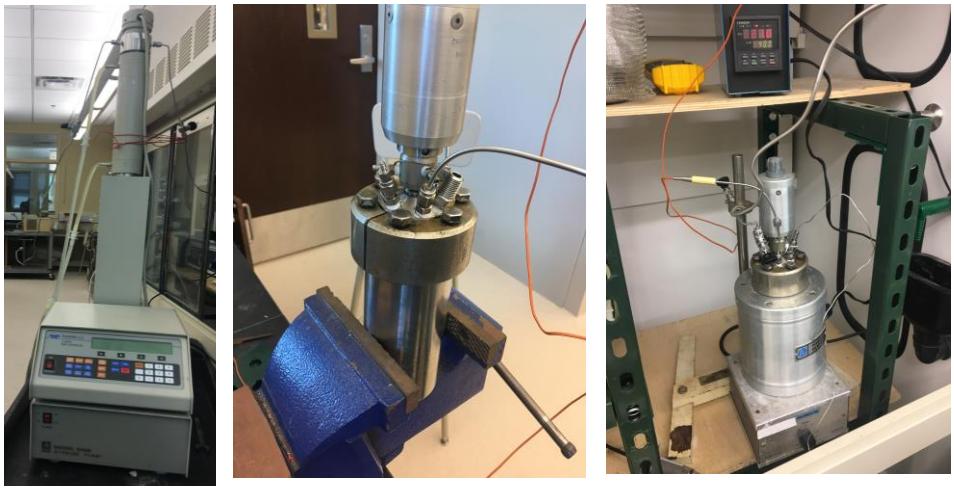

Figure 16.

The iPSCO piston pump (*left*) pushes the gas or SCF into the Parr reactor shown in the vice (*middle*). The reactor is then placed into a temperature-controlled jacket (*right*).

4.2.3 Preliminary Proof of Concept Experiments

4.2.3.1 Experiment 1: *Transfer from Solid to IL*

Two beakers were placed inside the reactor. One had a small solid clump of concentrated Disperse Orange dye. The other had a small amount of an IL called 1-Hexyl-3-methylimidazolium bis(trifluoromethylsulfonyl)imide (*Figure 17).* The reactor

was first heated to 40°C then was pressurized with CO_2 using an IPSCO piston pump. Once it was pressurized to 1450 psi, it was left for about a day before being removed and opened. The IL was successfully saturated with the dye (*Figure 17b*). Most solid dye was not consumed.

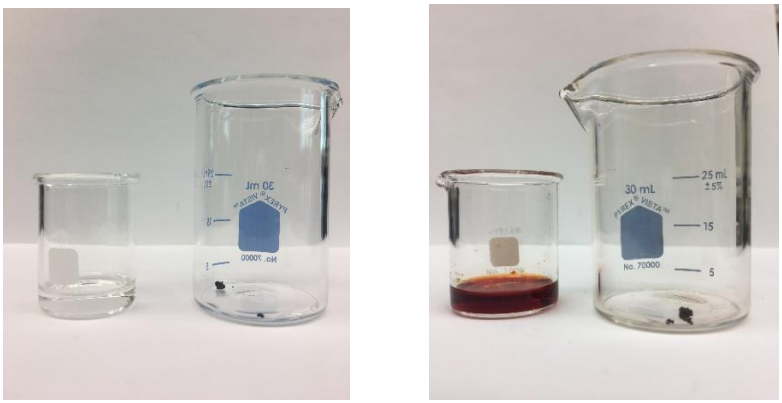

A B

Figure 17.

Before pressurization for experiment 1: The left is the clear IL and the right contains solid clumps of Disperse Orange *(A).* After pressurization for experiment 1: The left is the saturated IL and the right contains what is left of the solid clumps of Disperse Orange *(B).*

4.2.3.2 Experiments 2 through 4: *Transfer from IL to IL Series*

Experiments two through four (*Figure 18*) were all conducted to accomplish the same thing: transfer the dye particles from an IL pre-loaded with Disperse Orange to an IL of equivalent mass with no dye. Experiment 2 was pressurized for approximately four days, experiment 3 for only one day, and experiment 4 for two days. The third and fourth

experiments involved mixing each the ILs and the CO_2 itself. The UV-vis absorbance level of the sample IL (the one originally loaded with Disperse Orange, labelled “S”) was taken before pressurization and the absorbance levels of both the sample and the pure (IL with no preloaded Disperse Orange, labelled “P”) were taken after pressurization.

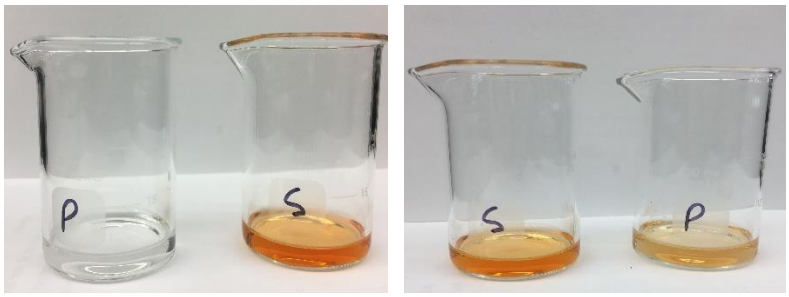

A B

C D

E F

Figure 18.

The before and after shots of experiments 2 (*A and B*), 3 (*C and D*) and 4 (*E and F*). The before pictures (*left of each set*) show the sample (orange) and pure (clear) beakers/vials before pressurization. The after pictures (*right of each set*) show the sample (orange) and pure (clear) beakers/vials after pressurization.

4.2.3.3 Experiment 5: *Transfer from Solid Mix to IL*

Two beakers were placed inside a pressure safe vessel. One contained a 1:4 solid mix of 0.0021 g Disperse Orange and 0.0063 g Methylene Blue. The other contained the clear IL used in previous experiments. It was pressurized to 1450 psi and left for a day. The dye and the IL reached equilibrium and the IL was saturated. *Figure 19* shows the results of this experiment.

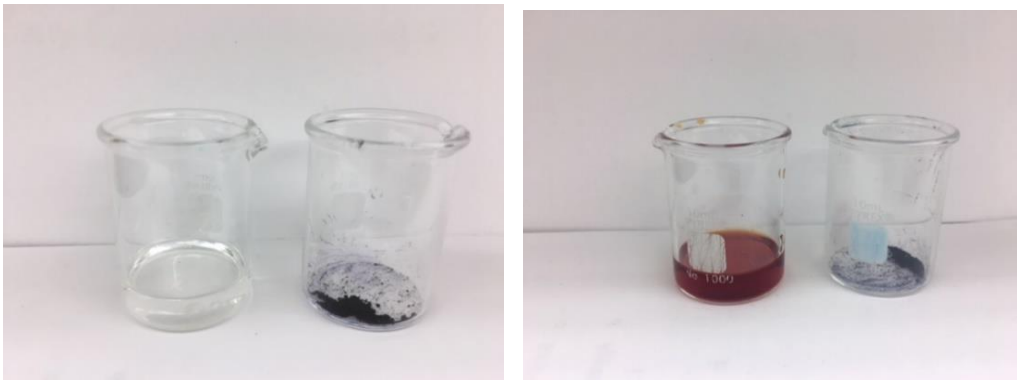

A B

Figure 19.

Before pressurization for experiment 5: On the left is the clear IL and the right contains solid mix of Methylene Blue and DO (*A*). After pressurization for experiment 5: On the left is the saturated IL and the right contains the remaining solid mix (*B*).

4.2.3.4 Experiment 6: *Co-Transfer of Citric Acid and Water*

One beaker containing 2.6212 g HPLC grade water and another beaker containing 0.6266 g solid citric acid were pressurized to 1450 psi at 40^{o}C for a day (*Figure 20a*). The water and citric acid successfully co-transferred (*Figure 20b*). Using pH strips (*Figure 21*), the water before pressurization was about 5.0. After pressurization, the water's pH was between 3.5 and 4. The pH of the water transferred to the beaker containing citric acid fell below 3.0 on the scale.

Figure 20.

Before pressurization for experiment 6: On the left is water and the right contains solid citric acid (*A*). After pressurization for experiment 6: The left beaker contains some water that had humidified and traveled to the beaker with the remaining solid acid and the right is the saturated water (*B*).

A B C

Figure 21.

Before pressurization for experiment 6: the starting pH of the water was 5.0 (*A*). After pressurization for experiment 6: The water (*B*) read approximately 3.75 and the water that traveled to the citric acid (*C*) read well below 3.0

4.2.3.5 Experiment 7: *Transfer from DO1 Soaked Filter Paper to IL*

One beaker containing 3.5897 g IL1 and a dried DO1-soaked filter paper pressurized to 1450 psi at 40^{o}C for a day (*Figure 22*). Once depressurized, the filter paper was slightly lighter in pigment and the IL contained hints of orange. DO1 successfully transferred to the IL.

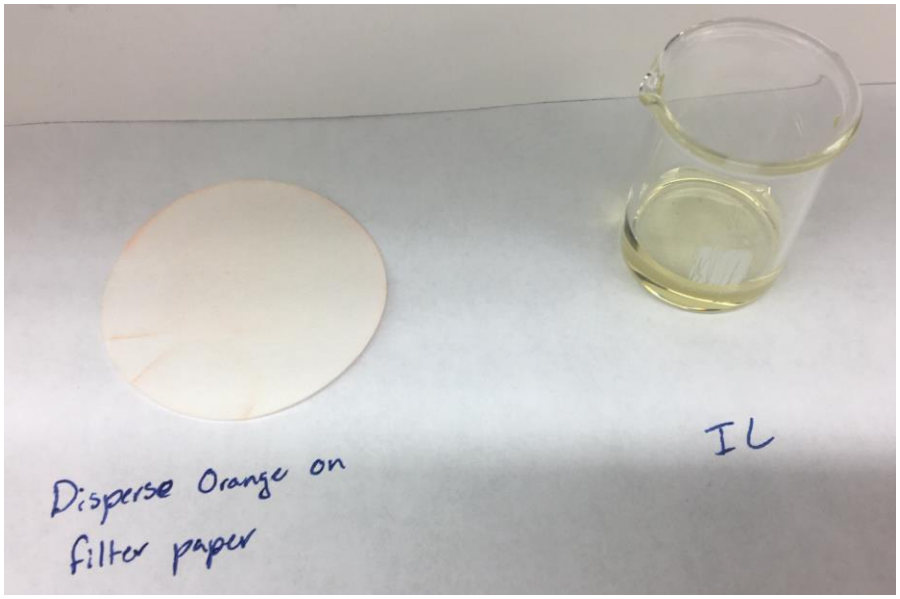

Figure 22.

After pressurization of experiment 7: the dye has faded on the filter paper and the IL has been tinged a light orange color

4.2.3.6 Experiment 8: *Selective Transfer of Solid DO1 to 2 Different ILs*

One vial containing 1.9596 g IL1 [methyl-2-hydroxyethylimidazolium bis((trifluoromethyl)sulfonyl)imide], another containing 1.9993 g IL2 [methyl-(2-oxyethyl) pyrrolidinium bis((trifluoromethyl)sulfonyl)imide] and a beaker with 0.0009 g of solid DO1 (*Figure 23a*) were pressurized to 1476 psi at 40oC for 48 hours. A small amount of pressure was lost due to a leak at the pressure sensor connection. At 48 hours, the pressure was still 1412 psi. IL1 was a noticeably darker orange than IL2 (*Figure 23b*).

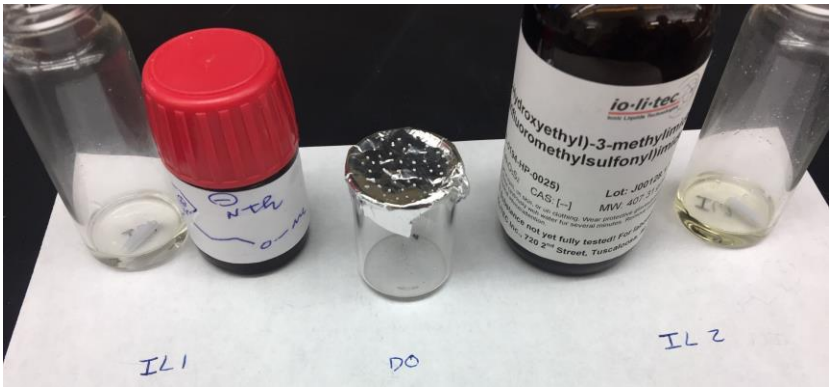

A

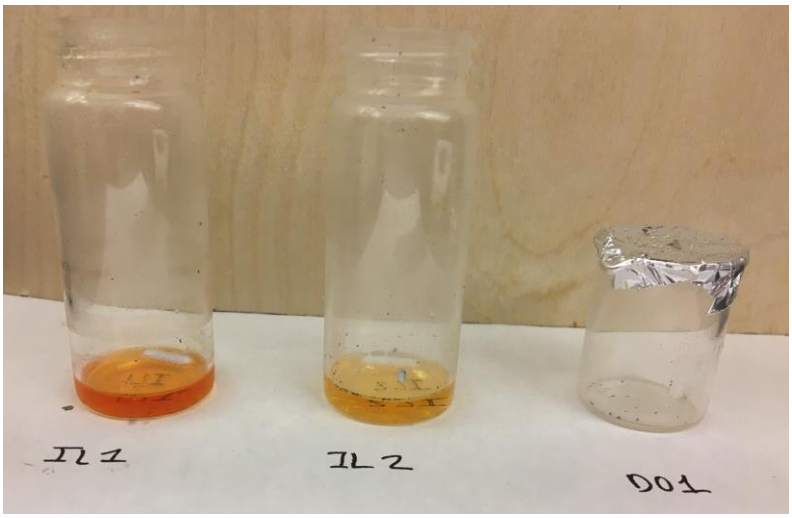

B

Figure 23.

Before pressurization for experiment 8: From left to right is the vial of IL1 sample, original container for IL1, small beaker with clump of DO1, original bottle of IL2, and vial of IL2 sample (*A*). After pressurization for experiment 8: visually, there the vial on the left (IL1) is much darker than the middle vial (IL2). The small beaker on the right contains the remains of the DO1. The metal flecks seen in the vials are aluminum foil specks that unintentionally transferred during pressurization of the system (*B*).

4.2.4 Experiments 9 through 13

Time Series for Transfer of Solid DO1 to 2 Different ILs

Each of the experiments in this series uses the same ILs (structures shown in *Figures 24 - 26*) at 40°C and relative procedure with the main difference being the time the reactor and its contents were left under pressure. There were also minor differences in the setup within the reactor to allow better circulation of the SCF as can be seen in section *4.2.8 Evolution of Experimental Setup*. Experiment 12 is a repeat of experiment 9 due to complications encountered when a connection was sheared off while contents were under pressure as well as a change in setup that reduced the IL surface area exposed to the CO_2. The pressure durations used were 6 hours (experiments 9 and 12), 12 hours (experiment 10), 3 hours (experiment 11), and 1.5 hours (experiment 13).

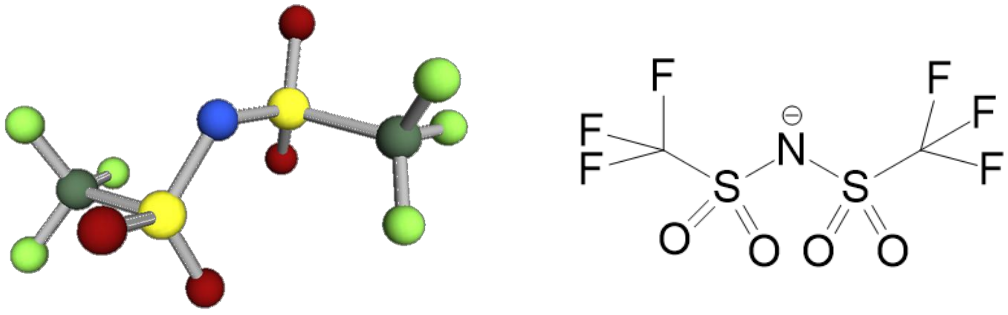

Figure 24.

The anion bis((trifluoromethyl)sulfonyl)imide is common between both IL1 and IL2. On the left is the gas phase geometry and the right displays the atomic makeup.

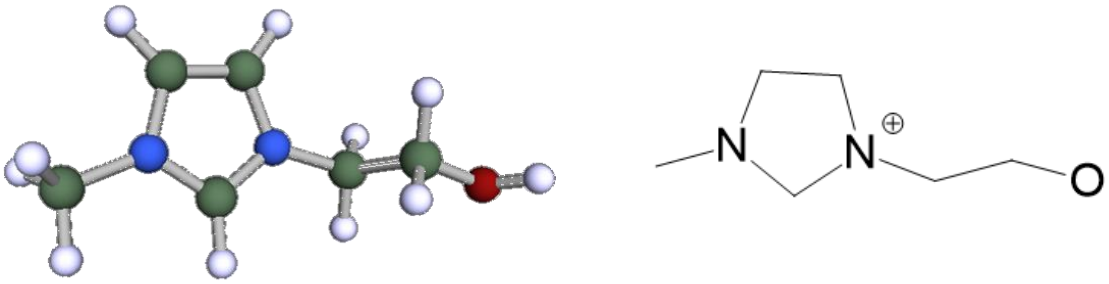

Figure 25.

The cation methyl-2-hydroxyethyl imidazolium is found only in IL1. On the left is the gas phase geometry and the right displays the atomic makeup.

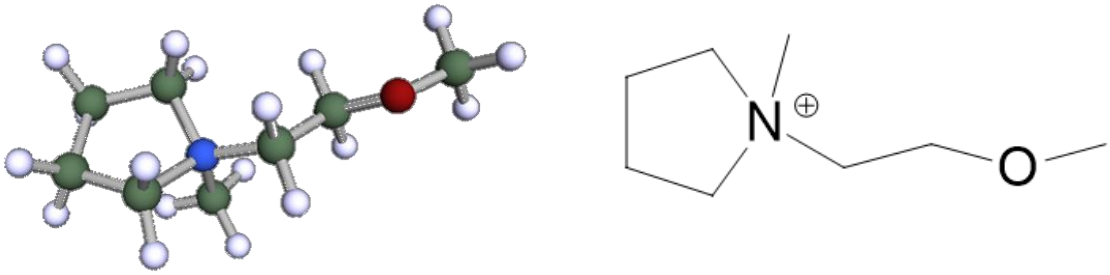

Figure 26.

The cation methyl-(2-methoxyethyl) pyrrolidinium is IL2's cation. On the left is the gas phase geometry and the right displays the atomic makeup.

Qualitative visual results for each can be seen in *Figure 27* and quantitative concentration data is represented in *Table 5*. UV-vis spectroscopy was used to obtain quantitative data for each. Beer-Lambert's law (*Equation 24*) was used to derive the concentration from the absorbance data at wavelength 450 nm. This equation equates absorbance of light (A) at the specified wavelength to the concentration of substance (c), the length (l) of the path the light takes through the substance and the molar absorptivity

(ϵ). However, since the length and the molar absorptivity remain nearly constant, they can be replaced with a fixed constant (k). When comparing the concentration of dye in IL1 to IL2, a ratio can be set up that will cancel out the fixed constant leaving only *Equation 25* to describe the comparison.

$$A = \epsilon c l = kc \qquad \textit{(Equation 24)}$$

$$\frac{A_1}{A_2} = \frac{C_1}{C_2} \qquad \textit{(Equation 25)}$$

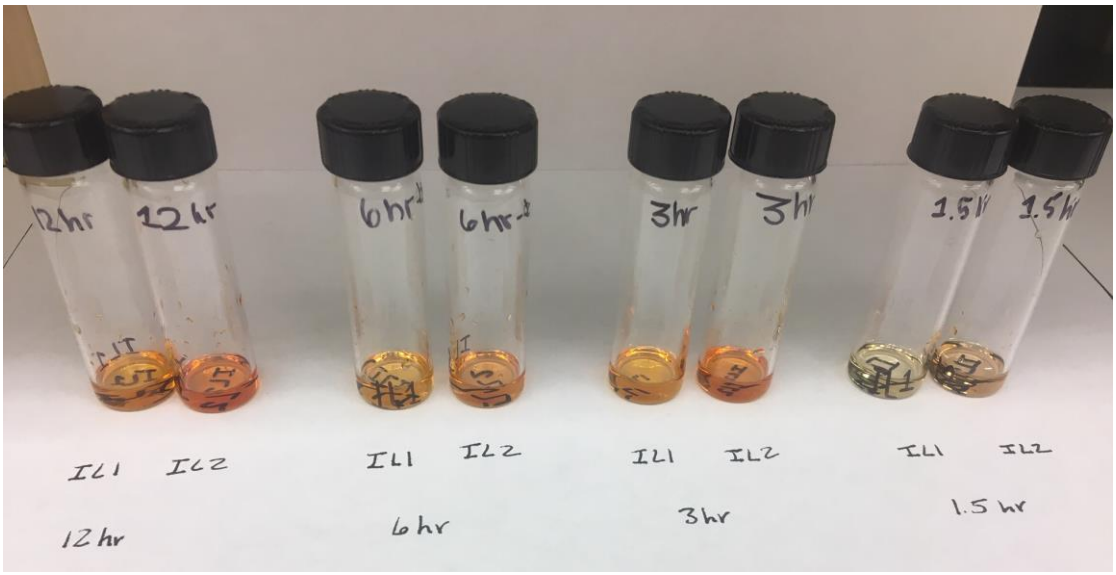

Figure 27.

Comparison of results from experiments 10-13: each pairing has IL1 on the left and IL2 on the right. Pairs from left to right belong to experiments 10 (12 hours), 12 (6 hours), 11 (3 hours) and 13 (1.5 hours)

4.2.5 Experiments 14 through 16

Temperature Series for Transfer of Solid DO1 to 2 Different ILs

The experiments in this series shares the same ILs and relative procedure with the experimental Time Series except that the temperature was raised to 60^{o}C. The experiments in this series are also conducted under different time durations like the Time series; however, the times used are 6 hr (Exp 14), 24 hr (Exp 15), and 1.5 hr (Exp 16). Again, Beer-Lambert's law was used to derive the concentration from the absorbance data at wavelength 450 nm. The results can be seen in *Figure 28* and *Table 5*.

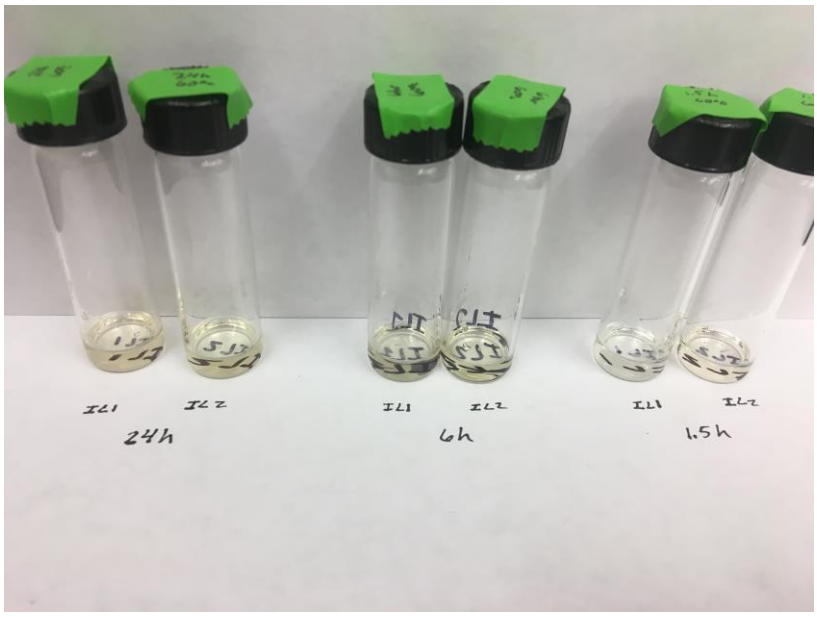

Figure 28.

Comparison of results from experiments 14-16: each pairing has IL1 on the left and IL2 on the right. Pairs from left to right belong to experiments 15 (24 hours), 14 (6 hours) and 16 (1.5 hours)

4.2.6 Discussion of Experiments 10 through 16

As expected, the longer the system was allowed to reach equilibrium, the higher the uptake of DO1. Though, there is greater difference between the shorter time frames than longer ones that have been allowed to reach or almost reach complete equilibrium. On the other hand, raising the temperature by 20 degrees has a tremendous adverse effect on transfer. Going back to *Equation 23,* the mole fraction of solute in the solution is inversely related to pressure. Increasing the temperature increases the pressure proportionately thereby decreasing the mole fraction. In 24 hours at the higher temperature, the concentration is barely able to be seen as even a tint to the IL.

The interesting result is that even though it can visually be seen that IL2 is darker orange than IL1 in each set of vials in *Figure 29* strongly suggesting it has the higher concentration of dye, the calculated concentration ratios (shown in the last column of *Table 5*) are split on their results. Experiments 10, 12, and 13 have ratios equal to less than 1 meaning the dye favored IL2 which agrees with the qualitative results. Conversely, experiments 11, 14, 15, and 16 have ratios greater than 1 in favor of IL1 being the recipient of more dye. Some reasons for this could be that there were, in fact, differences in the molar absorptivity or in the viscosity of the ILs at different temperatures. If the molar absorptivity varies between the ILs then there is not a direct proportionality between the absorbance and the concentration. Also, if the viscosity of the ILs is the limiting factor, perhaps leaving the system under pressure for a greater length of time will produce more consistent data. These two ILs were picked as they were readily available and had different cations that featured differing functional groups that were expected to

exhibit selectivity such as IL1 being an imidazolium with a hydroxyl group and the other a pyrrolidinium without one. Further research is required to explore the results.

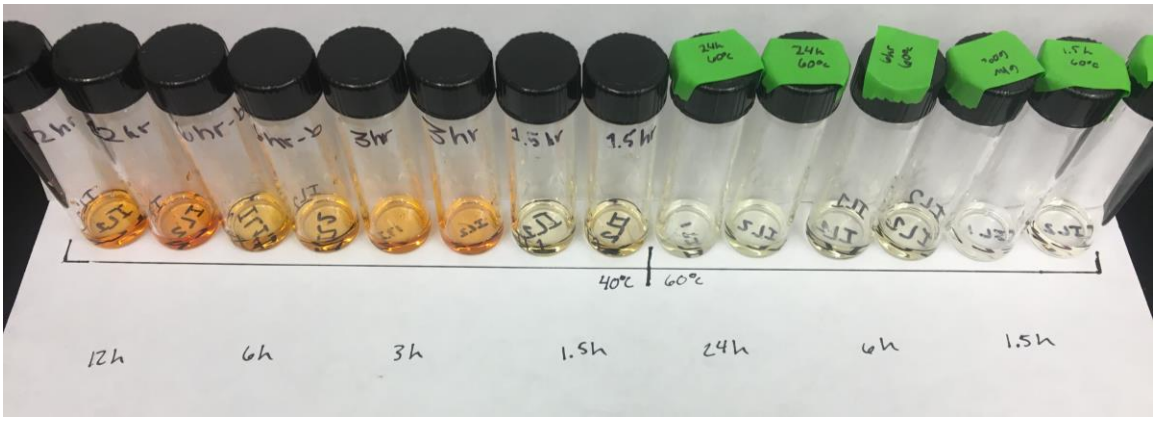

Figure 29.

Comparison of results from experiments 10-16: each pairing has IL1 on the left and IL2 on the right. Pairs from left to right belong to experiments 10 (12 hours, 40°C), 12 (6 hours, 40°C), 11 (3 hours, 40°C), 13 (1.5 hours, 40°C), 15 (24 hours, 60°C), 14 (6 hours, 60°C) and 16 (1.5 hours, 60°C)

Table 5. Relative Average Absorbance of DO1 (*at wavelength 450 nm)

Exp #	Time (h)	Temp (C)	A_1 (IL1)	A_2 (IL2)	C_1/C_2
10	12	40	0.561	0.626	0.90
11	3	40	0.864	0.439	1.97
12	6	40	0.617	0.659	0.94
13	1.5	40	0.345	0.489	0.71
14	6	60	0.344	0.249	1.38
15	24	60	0.401	0.292	1.37
16	1.5	60	0.198	0.168	1.18

4.2.7 Evolution of Experimental Setup

The preliminary experiments also served as testing grounds for how to maximize the efficiency of flow within the reactor by adjusting the placement of the containers and adding stirring of the contents. How the experiments were setup within the reactor were varied multiple times. Some of these adjustments were to better space out the vials and beaker. Others were to allow for more or improved circulation of the SCF.

Initial design (*Figure 30 left*) of the placing only required two beakers: one to contain the solid DO1 and one for the IL. The IL beaker was placed on top of a slightly larger beaker at an angle to allow the SCF to access the DO1 with less probability of displacement from wind created by possible rapid fluctuations in pressure at initial filling and releasing of the SCF. Experiment 2's placement (*Figure 30 right*) was basically the same with the only difference being that the DO1 was not in solid form but premixed into the IL.

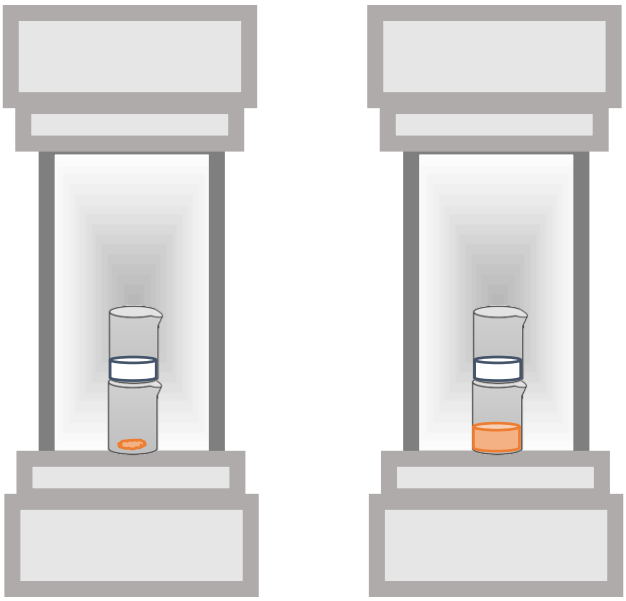

A B

Figures 30.

Both diagrams show the initial set up inside of the reactor before pressurization. The IL is the white substance in the top beaker and the orange is the Disperse Orange I in solid form (*A*) and liquid form (*B*)

For the next two experiments (*Figure 31)*, stirring was introduced not only in the ILs but also in the SCF. An empty vial was added just to stabilize the other two vials. Aluminum foil was folded into a 1-inch strip then curled to tuck into itself to form a ring large enough for a stir bar to rotate within it with a circle of mesh wire covering it to provide a platform on which to place the vials.

Figures 31.

The picture on the left shows the diagram of the actual setup shown on the right

Modified from those, experiments 5 and 6 used a modified placement resembling both previous setups (*Figure 32 left*). One small beaker containing an IL was set above another beaker of powdered solid. In addition to the aluminum foil ring and mesh wire being used to make room for a stir bar to mix the SCF, the wire was also used to stabilize the small beakers to prevent tipping or spilling of their contents (*Figure 32 right*).

Figure 32.

The picture on the left shows the diagram of the actual setup for experiments 5 and 6 shown on the right

Since experiment 7 is transferring the DO1 from filter paper, a new setup to prevent the paper from moving around the reactor was needed (*Figure 33a*). So, the wire mesh was placed above the beaker of IL to both support and weigh down the saturated filter paper (*Figure 33b*).

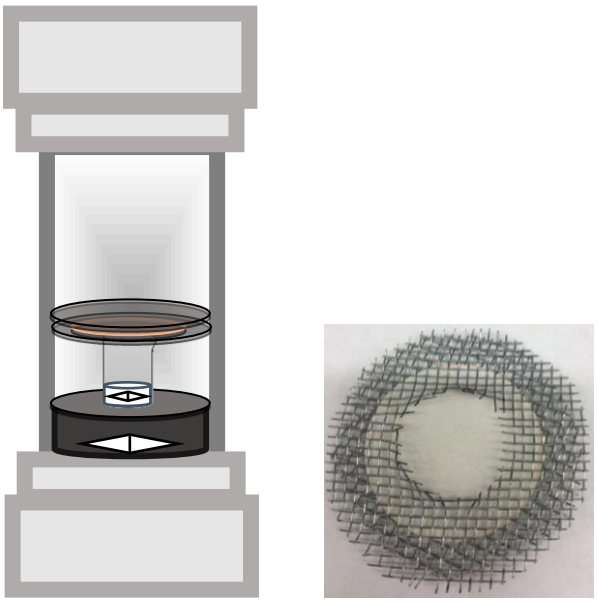

Figure 33.

A diagram of experiment 7 (*A*) which used a clean filter paper sandwiched between two mesh wire circles as shown in *B.*

CHAPTER V

CONCLUSIONS AND FUTURE DIRECTIONS

5.1 Conclusions

This work was started to explore ways to enhance traditional extraction methods using supercritical fluids in combination with ionic liquids (ILs) or other nonvolatile liquids. Two modeling methods were developed and validated. One used Excel's Visual Basic Applications (VBA) to test solubilities in supercritical fluids. The other used the conductor-like screening model for real solvents (COSMO-RS) to screen through various combinations of anions and cations to form an effective ionic liquid or a pair of contrasting ionic liquids. Along with the modeling methods, preliminary experiments were used to demonstrate proof of concept experimental extractions.

Solubility modeling was used to better understand the behavior and tunability of SCFs and how temperature or pressure changes would affect the solubility of a solute into it. The Peng-Robinson EoS was used for its accuracy and simplicity of calculations.

COSMO modeling accurately predicted the same behavior seen by West et al. (4) in their work on dyeing a polymer with supercritical carbon dioxide. This modeling method also screened through a selection of cations and anions pairings for the selectivity of the dyes used in that same work. It was found for this system that the anion selection

made more of an impact than the cation, because the "hardness" of the anion, or how dense the charge, determined how strong the interactions with the hydroxyl group on the DR1 was.

Several preliminary experiments were conducted to prove this method and the fundamental theories behind it. Most of these aimed to transfer Disperse Orange I (DO1) dye into an IL or to selectively transfer the dye to one IL over another. Following those, two series of experiments were conducted to observe the effects time and temperature have on the system.

The effect seen from varying times and temperatures verified that longer durations allowed time for the system to reach equilibrium though there was less drastic difference in results between times once equilibrium had been mostly achieved. The payoff between the cost of time and the marginal boost in quality would need to be evaluated on a system-to-system basis.

Increasing the temperature further above the critical point hindered the transfer of material. This could possibly be due to the solute's affinity for the SCF becoming greater than its affinity for the ILs available. For these experiments, the optimal temperature was just above the critical point for the supercritical fluid to function in the zone where it behaves like both gases and liquids.

5.2 Future Directions

ILESCFE potentially has countless future applications because of the versatility and tunability of ionic liquids and supercritical fluids. Just about anywhere that extraction of a solute or impurity is needed, there is the possibility for this method to

enhance it. Not every possibility will see improvement upon current methods, but ultimately it will not be known until further investigation. Such investigation as will be accomplished under the NSF proposal this research was conducted for. Two projects, in particular, have some foundation to build from as laid out in this thesis.

5.3 Pharmaceutical Application

Every year the influenza virus takes many lives and leaves many with serious illness. Tamiflu® (Oseltamivir by generic name) is a neuraminidase inhibitor that is used as an antiviral medication and is produced by Roche laboratories. While this drug has not been seen to be effective for the COVID pandemic, it was successful as treatment of the 2009 swine flu (H1N1) pandemic and to a lesser extent, the 2006 avian flu (H5N1) pandemic. If administered to an influenza patient within a short time after symptoms begin (~36 hours), the severity of symptoms is reduced and symptom duration is shortened by up to a day (14). The main limiter in large-scale production is acquiring the synthetic precursors of the drug. Shikimic acid is one of two main precursors of this antiviral medication, so it is sensible to find ways to more effectively and efficiently extract it from star anise seeds from which it is sourced (15).

5.4 Archeological Application

The other application is a project to identify the source of pottery stains in such a manner as to not damage the pottery itself. This project is specific to pottery sherds colored by “black drink” - stains derived from either coffee or cocoa beans. Coffee and cocoa beans were once used as the primary sources of coloring pottery at different times.

ILESCFE can be used to selectively collect the caffeine and theobromine out of the sherds into separate ILs to then see the concentration of each solute in the original pottery. The difference in caffeine and theobromine concentrations can establish the source of the coloration since coffee has a higher caffeine content and chocolate has a higher theobromine level. This will help archeologists to determine the period in which the pottery was made.

REFERENCES

1. Taylor, Larry T. *Supercritical Fluid Extraction*. Wiley-Interscience, 1996.

2. Freemantle, Michael. *An Introduction to Ionic Liquids*. RSC Publishing, 2010.

3. Freire, Mara G., et al. "Evaluation of COSMO-RS for the Prediction of LLE and VLE of Water and Ionic Liquids Binary Systems." *Fluid Phase Equilibria*, vol. 268, no. 1–2, June 2008, pp. 74–84. *Crossref*, https://doi.org/10.1016/j.fluid.2008.04.009.

4. West, Barry, et al. "Supercritical Fluid Dyeing of PMMA Films with Azo-Dyes."*Journal of Applied Polymer Science*, vol. 69, 1998, pp. 911–19.

5. Blanchard, Lynnette A., and Joan F. Brennecke. "Recovery of Organic Products from Ionic Liquids Using Supercritical Carbon Dioxide." *Industrial & Engineering Chemistry Research*, vol. 40, no. 1, Jan. 2001, pp. 287–92. *Crossref*, https://doi.org/10.1021/ie000710d.

6. Klamt, Andreas, and Frank Eckert. "COSMO-RS: A Novel and Efficient Method for the a Priori Prediction of Thermophysical Data of Liquids." *Fluid Phase Equilibria*, vol. 172, no. 1, July 2000, pp. 43–72. *Crossref*, https://doi.org/10.1016/S0378-3812(00)00357-5.

7. Eckert, Frank, and Andreas Klamt. "Validation of the COSMO-RS Method: Six Binary Systems." *Industrial & Engineering Chemistry Research*, vol. 40, no. 10, May 2001, pp. 2371–78. *Crossref*, https://doi.org/10.1021/ie0009132.

8. Klamt, Andreas. "Conductor-like Screening Model for Real Solvents: A New Approach to the Quantitative Calculation of Solvation Phenomena." *The Journal of Physical Chemistry*, vol. 99, no. 7, Feb. 1995, pp. 2224–35. *DOI.org (Crossref)*, https://doi.org/10.1021/j100007a062.

9. Peng, Ding-Yu, and Donald B. Robinson. "A New Two-Constant Equation of State." *Industrial & Engineering Chemistry Fundamentals*, vol. 15, no. 1, Feb. 1976, pp. 59–64. *Crossref*, https://doi.org/10.1021/i160057a011.

10. Shinoda, Takashi, and Kazuhiro Tamura. “Solubilities of C.I. Disperse Red 1 and C.I. Disperse Red 13 in Supercritical Carbon Dioxide.” *Fluid Phase Equilibria*, vol. 213, no. 1, Oct. 2003, pp. 115–23. *ScienceDirect*, https://doi.org/10.1016/S0378-3812(03)00240-1.

11. Tamura, Kazuhiro, and Takashi Shinoda. “Binary and Ternary Solubilities of Disperse Dyes and Their Blend in Supercritical Carbon Dioxide.” *Fluid Phase Equilibria*, Molecular Thermodynamics and Molecular Simulation, 219, no. 1 (May 10, 2004): 25–32. https://doi.org/10.1016/j.fluid.2004.01.009.

12. Liu, Dehua, et al. “CO2-Induced PMMA Swelling and Multiple Thermodynamic Property Analysis Using Sanchez−Lacombe EOS.” *Macromolecules*, vol. 38, no. 10, American Chemical Society, May 2005, pp. 4416–24. *ACS Publications*, https://doi.org/10.1021/ma047319e.

13. Li, Shufen, et al. “Solubilities of Theobromine and Caffeine in Supercritical Carbon Dioxide: Correlation with Density-Based Models.” *Fluid Phase Equilibria*, vol. 68, Nov. 1991, pp. 263–80. *ScienceDirect*, https://doi.org/10.1016/0378-3812(91)85023-N.

14. *A New Ion Selective Electrode Method for Determination of Oseltamivir Phosphate (Tamiflu) and Its Pharmaceutical Applications | Elsevier Enhanced Reader*. https://doi.org/10.1016/j.arabjc.2012.07.029. Accessed 7 Aug. 2021.

15. Farina, Vittorio, and Jack D. Brown. “Tamiflu: The Supply Problem.” *Angewandte Chemie International Edition*, vol. 45, no. 44, 2006, pp. 7330–34. *Wiley Online Library*, https://doi.org/10.1002/anie.200602623.

APPENDICES

Appendix A

Excel Visual Basics Applications Code for Solubility Modeling

```
' orginal PREOS with quadratic mixing rules and linear combining rules
' two interatction parameters, one for amix and one for bmix

Public Const omega = 0.0778, psi = 0.45724, R = 83.14
Function ai(T As Double, tc As Double, pc As Double, w As Double) As Double
   Dim tr As Double, alpha As Double
   tr = T / tc
   alpha = (1 + (0.37464 + 1.54226 * w - 0.26992 * w ^ 2) * (1 - Sqr(tr))) ^ 2
   ai = psi * alpha * R ^ 2 * tc ^ 2 / pc
End Function

Function bi(tc As Double, pc As Double) As Double
   bi = omega * R * tc / pc
End Function

Function qi(a As Double, b As Double, T As Double) As Double
  qi = a / b / R / T
End Function

Function Psat(a As Double, b As Double, c As Double, T As Double) As Double    'bar
   Psat = (10 ^ (a - (b / (c + T - 273.15)))) / 750.06
End Function

Function beta(b As Double, P As Double, T As Double) As Double
   beta = b * P / R / T
End Function

Function IPREOS(z As Double, beta As Double) As Double
   sigma = 1 + Sqr(2)
   epsilon = 1 - Sqr(2)
   IPREOS = 1 / (sigma - epsilon) * WorksheetFunction.Ln((z + sigma * beta) / (z + epsilon * beta))
End Function
```

```
Function zPR(T As Double, P As Double, tc As Double, pc As Double, w As Double, phase As
Integer) As Double
   Dim aii As Double, bii As Double, beta As Double, q As Double
   Dim AA As Double, BB As Double, CC As Double, KK As Double, LL As Double, MM As Double
   Dim theta As Double, z(1 To 3) As Double
   Dim zL As Double, zV As Double
   Dim s As Double, e As Double
   s = 1 + Sqr(2)
   e = 1 - Sqr(2)
   aii = ai(T, tc, pc, w)
   bii = bi(tc, pc)
   beta = bii * P / R / T
   q = aii / bii / R / T
   AA = (s + e - 1) * beta - 1
   BB = (s * e - s - e) * beta ^ 2 + (q - s - e) * beta
   CC = -(s * e * (1 + beta) + q) * beta ^ 2
   KK = (AA ^ 2 - 3 * BB) / 9
   LL = (2 * AA ^ 3 - 9 * AA * BB + 27 * CC) / 54
   MM = LL ^ 2 - KK ^ 3

   If MM > 0 Then
      zPR = WorksheetFunction.Power(-LL + Sqr(MM), 1 / 3) + WorksheetFunction.Power(-LL -
Sqr(MM), 1 / 3) - AA / 3
   Else
      theta = WorksheetFunction.Acos(LL / Sqr(KK ^ 3))
      z(1) = -2 * Sqr(KK) * Cos(theta / 3) - AA / 3
      z(2) = -2 * Sqr(KK) * Cos((theta + 2 * WorksheetFunction.Pi()) / 3) - AA / 3
      z(3) = -2 * Sqr(KK) * Cos((theta - 2 * WorksheetFunction.Pi()) / 3) - AA / 3
      zL = WorksheetFunction.Min(z)
      zV = WorksheetFunction.Max(z)

      If phase = 0 Then
         zPR = zL
      Else
         zPR = zV
      End If
   End If
End Function

Function phiSat(beta As Double, z As Double, q As Double, i As Double) As Double
   phiSat = Exp(z - 1 - WorksheetFunction.Ln(z - beta) - q * i)
End Function

Function aMix(y1 As Double, a1 As Double, a2 As Double, kij As Double) As Variant
   a12 = Sqr(a1 * a2) * (1 - kij)
```

```
   aMix = y1 ^ 2 * a1 + (1 - y1) ^ 2 * a2 + 2 * y1 * (1 - y1) * a12
End Function

Function bmix(y1 As Double, b1 As Double, b2 As Double) As Variant
   bmix = y1 * b1 + (1 - y1) * b2
End Function

Function zPRmix(beta As Double, q As Double, phase As Integer) As Double
  Dim z(1 To 3) As Variant
   s = 1 + Sqr(2)
   e = 1 - Sqr(2)
   AA = (s + e - 1) * beta - 1
   BB = (s * e - s - e) * beta ^ 2 + (q - s - e) * beta
   CC = -(s * e * (1 + beta) + q) * beta ^ 2
   KK = (AA ^ 2 - 3 * BB) / 9
   LL = (2 * AA ^ 3 - 9 * AA * BB + 27 * CC) / 54
   MM = LL ^ 2 - KK ^ 3

   If MM > 0 Then
      zPRmix = WorksheetFunction.Power(-LL + Sqr(MM), 1 / 3) + WorksheetFunction.Power(-LL -
Sqr(MM), 1 / 3) - AA / 3
   Else
      theta = WorksheetFunction.Acos(LL / Sqr(KK ^ 3))
      z(1) = -2 * Sqr(KK) * Cos(theta / 3) - AA / 3
      z(2) = -2 * Sqr(KK) * Cos((theta + 2 * WorksheetFunction.Pi()) / 3) - AA / 3
      z(3) = -2 * Sqr(KK) * Cos((theta - 2 * WorksheetFunction.Pi()) / 3) - AA / 3
      zL = WorksheetFunction.Min(z)
      zV = WorksheetFunction.Max(z)

      If phase = 0 Then
         zPRmix = zL
      Else
         zPRmix = zV
      End If
   End If

End Function
Function a1bar(a1 As Double, a2 As Double, y1 As Double, aMix As Double, kij As Double) As
Double
   a12 = Sqr(a1 * a2) * (1 - kij)
   a1bar = 2 * y1 * a1 + 2 * (1 - y1) * a12 - aMix
End Function
Function b1bar(b1 As Double, b2 As Double, y1 As Double, bmix As Double) As Double
   b12 = 0.5 * (b1 + b2)
   b1bar = 2 * y1 * b1 + 2 * (1 - y1) * b12 - bmix
End Function
```

```
Function q1bar(aMix As Double, bmix As Double, a1bar As Double, b1bar As Double, qmix As
Double) As Variant
   q1bar = qmix * (1 + a1bar / aMix - b1bar / bmix)
End Function

Function phi_i_mix(z As Double, beta As Double, qibar As Double, bibar As Double, bmix As
Double) As Double
   sigma = 1 + Sqr(2)
   epsilon = 1 - Sqr(2)
   i = 1 / (sigma - epsilon) * WorksheetFunction.Ln((z + sigma * beta) / (z + epsilon * beta))
   phi_i_mix = Exp(bibar / bmix * (z - 1) - WorksheetFunction.Ln(z - beta) - qibar * i)
End Function

Function PoyntingFactor(V As Double, P As Double, Psat As Double, R As Double, T As Double) As
Double
   PoyntingFactor = Exp(V * (P - Psat) / R / T)
End Function

Function EnhancementFactor(phiSat As Double, PF As Double, PhiVap As Double) As Double
   EnhancementFactor = phiSat * PF / PhiVap
End Function
```

Appendix B

Aspen Plus V09 Shikimic Acid Properties Estimation

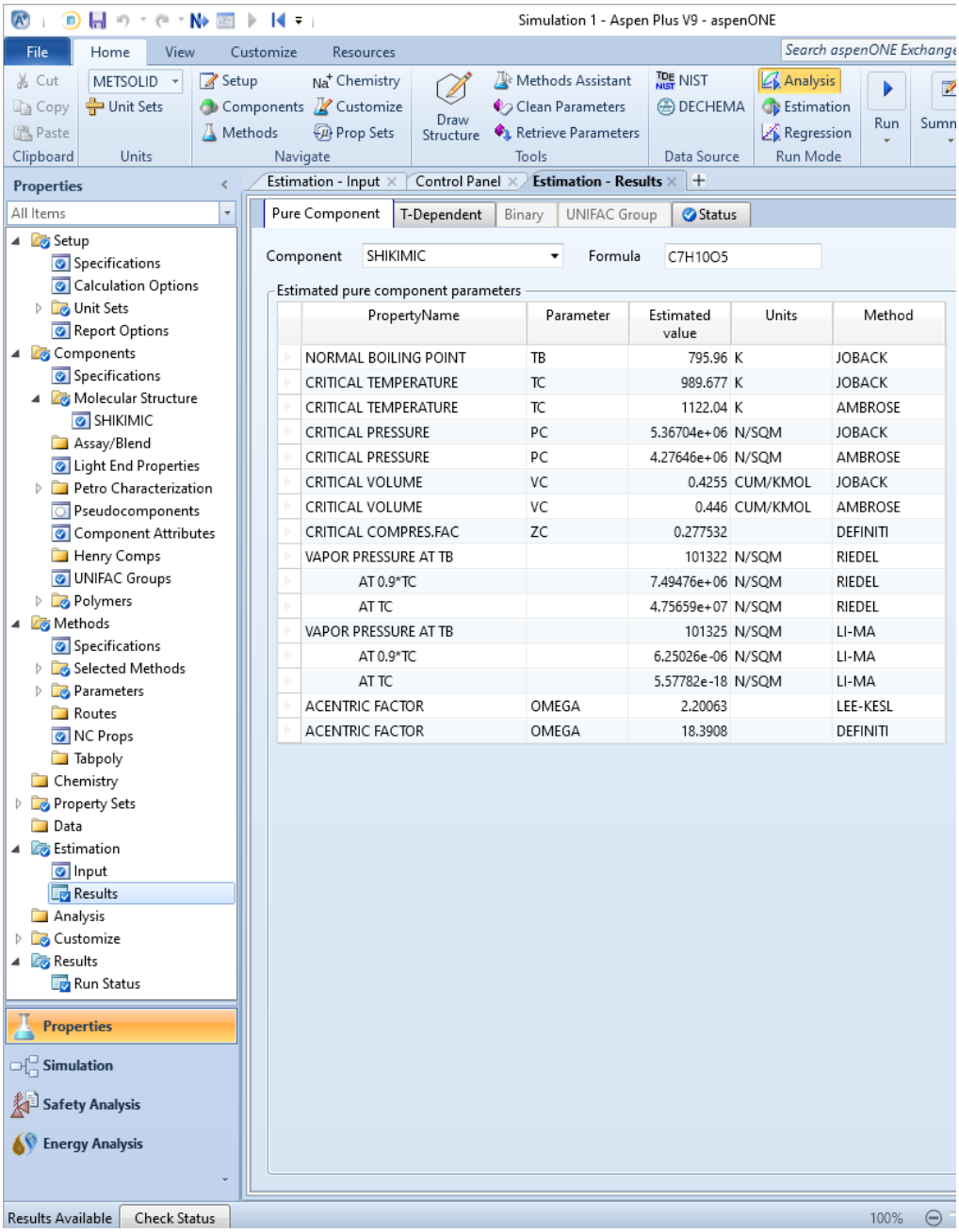

Figure 34.

Estimated pure component properties of shikimic acid given by Aspen Plus V9.

Appendix C

UV- *vis* Spectroscopy Relative Absorbance Data

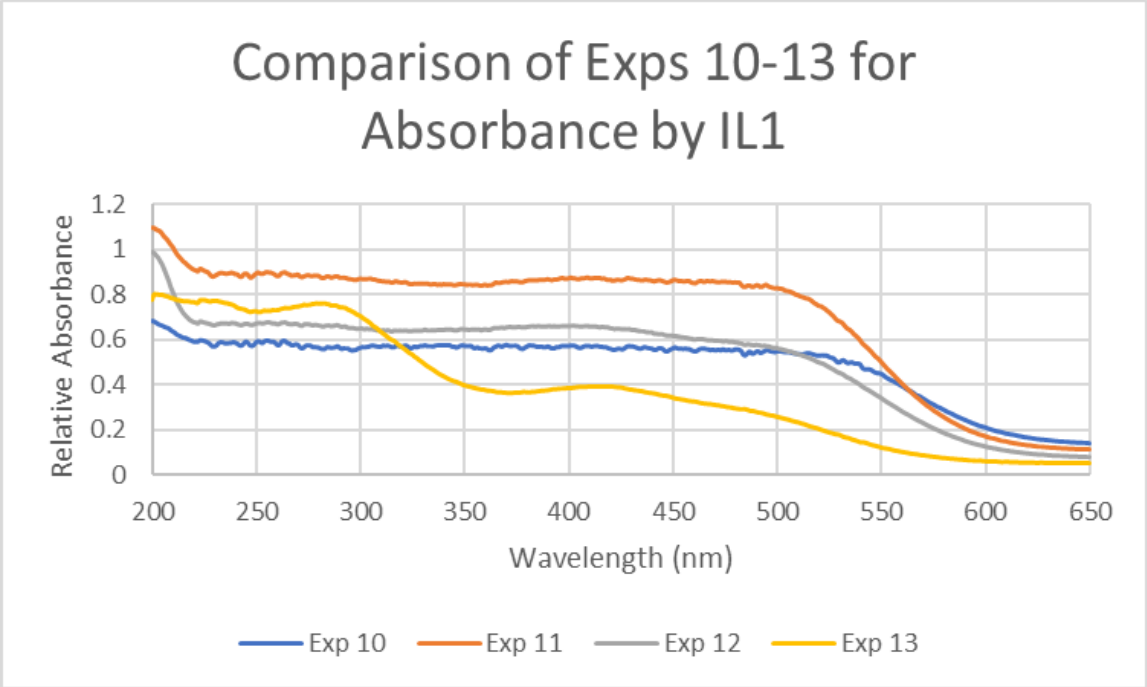

Figure 35.

UV- vis spectroscopy relative absorbance data for experiments 10 through 13 for the absorbance of light by IL1.

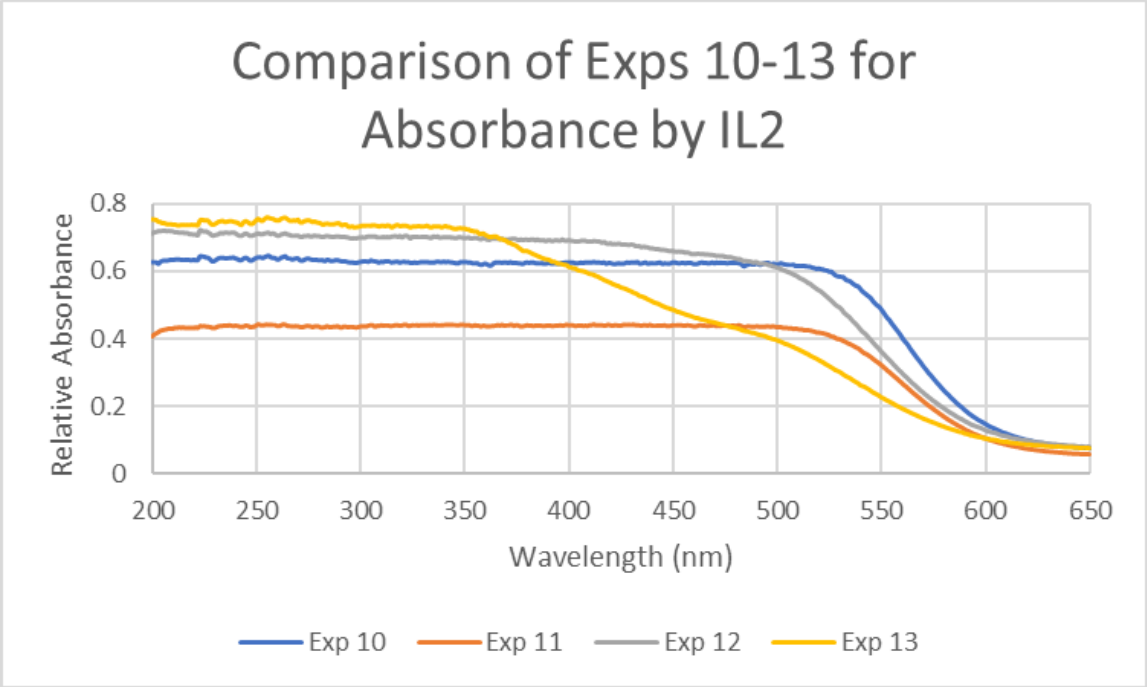

Figure 36.

UV- vis spectroscopy relative absorbance data for experiments 10 through 13 for the absorbance of light by IL2.

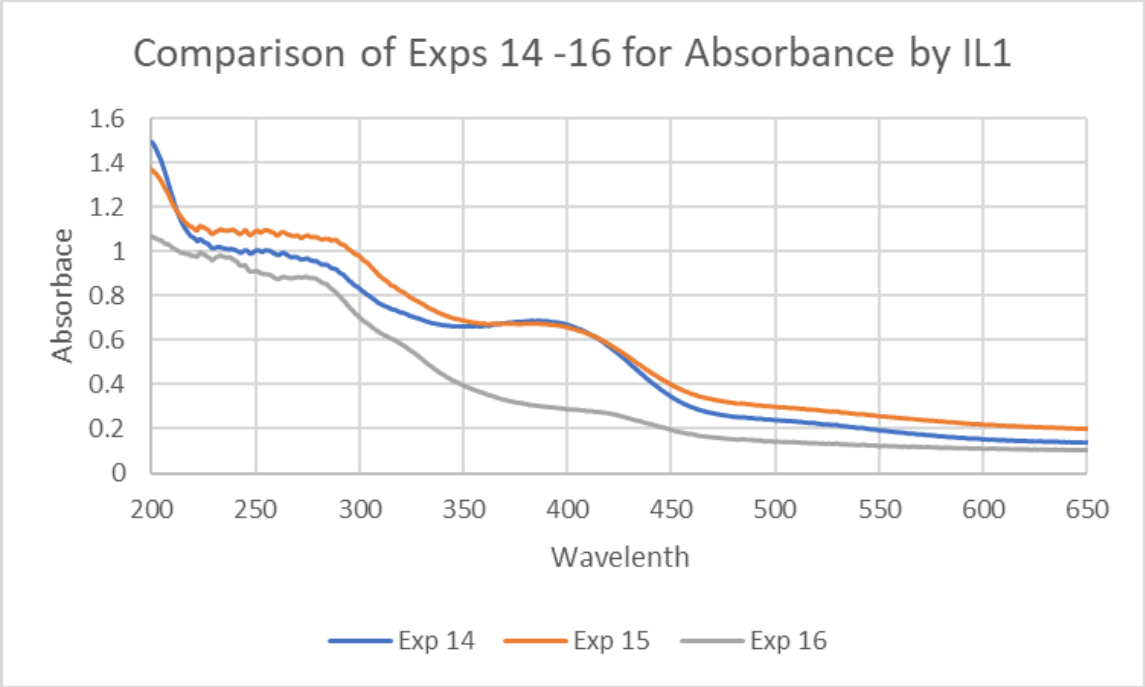

Figure 37.

UV- vis spectroscopy relative absorbance data for experiments 14 through 16 for the absorbance of light by IL1.

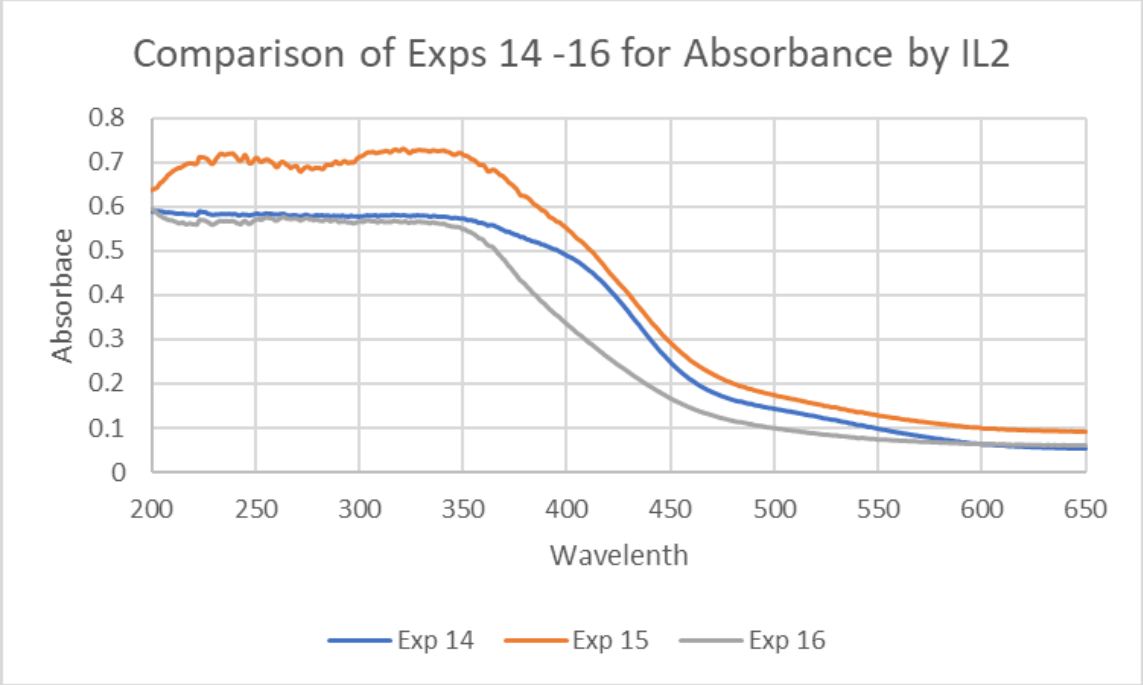

Figure 38.

UV- vis spectroscopy relative absorbance data for experiments 14 through 16 for the absorbance of light by IL2.

BIOGRAPHICAL SKETCH

Name of Author: Kelsey Tootle

Graduate and Undergraduate Schools Attended:

University of South Alabama, Mobile, Alabama

Degrees Awarded:

Bachelor of Science in Chemical Engineering, 2018
Master of Science in Chemical Engineering, 2021

Awards and Honors:

Graduate Research and Teaching Assistantship, Department of Chemical Engineering, 2018 - 2021